

GEODESIC SYNTHETIC CONTROL METHODS FOR RANDOM OBJECTS AND FUNCTIONAL DATA

DAISUKE KURISU*, YIDONG ZHOU*, TAISUKE OTSU, AND HANS-GEORG MÜLLER

ABSTRACT. We introduce a geodesic synthetic control method for causal inference that extends existing synthetic control methods to scenarios where outcomes are elements in a geodesic metric space rather than scalars. Examples of such outcomes include distributions, compositions, networks, trees and functional data, among other data types that can be viewed as elements of a geodesic metric space given a suitable metric. We extend this further to geodesic synthetic difference-in-differences that builds on the established synthetic difference-in-differences for Euclidean outcomes. This estimator generalizes both the geodesic synthetic control method and a previously proposed geodesic difference-in-differences method and exhibits a double robustness property. The proposed geodesic synthetic control method is illustrated through comprehensive simulation studies and applications to the employment composition changes following the 2011 Great East Japan Earthquake, and the impact of abortion liberalization policy on fertility patterns in East Germany. We illustrate the proposed geodesic synthetic difference-in-differences by studying the consequences of the Soviet Union’s collapse on age-at-death distributions for males and females.

1. INTRODUCTION

Since the seminal work by [Abadie and Gardeazabal \(2003\)](#) and [Abadie et al. \(2010\)](#), synthetic control methods (SCMs) have been widely applied to evaluate causal effects of policy changes in settings with observational panel or longitudinal data. SCMs are designed for settings where some units are subject to a policy intervention while others are not, and their outcomes are observed before and after the intervention. In such settings, synthetic control units constructed utilizing some optimal weighting of control units are employed to control for unobserved trends in the outcome over time that are unrelated to the policy effect. The SCM has become popular in many areas and has been applied in various comparative case studies of policy interventions (see [Abadie \(2021\)](#) for a survey).

Following the above pioneering work, the SCM has been extended in various directions, including an SCM that incorporates a penalty term for pairwise matching discrepancies between the treated units and the control units ([Abadie and L’Hour, 2021](#)), a SCM for high-dimensional settings ([Robbins et al., 2017](#)), a connection with matrix completion methods ([Amjad et al., 2018](#)) and conformal inference and robust t -testing for SCMs ([Chernozhukov et al., 2021a,b](#)). A modification of the synthetic control estimator by incorporating a bias correction method for inexact matching was proposed by [Ben-Michael et al. \(2021\)](#) and for a staggered adoption setting by [Ben-Michael et al.](#)

*The first two authors contributed equally to this work and are listed alphabetically.

Key words and phrases. causal inference, distributions, Fréchet mean, geodesic metric space, networks, synthetic difference-in-differences

MSC2020 subject classifications: 62D20, 62R20.

The work of D. K. was partially supported by JSPS KAKENHI Grant Number 23K12456 and the work of H.G.M. was partially supported by NSF grant DMS-2310450.

(2022), while Arkhangelsky et al. (2021) introduced a synthetic difference-in-differences (SDID) estimator that combines attractive features of the SCM and difference-in-differences (DID).

However, all of these developments primarily focused on Euclidean outcomes. In modern data analysis, one frequently encounters outcomes that may be inherently non-Euclidean, including distributional data (Petersen and Müller, 2016; Panaretos and Zemel, 2020; Petersen et al., 2022), compositional data (Scealy and Welsh, 2011), manifold-valued data (Patrangenaru and Ellingson, 2015), networks (Severn et al., 2022; Zhou and Müller, 2022) and functional data (Hsing and Eubank, 2015; Wang et al., 2016). Such data reside naturally in metric spaces where one often imposes additional mild properties such as geodesicity, which is satisfied for nearly all outcomes of interest, including those mentioned above under appropriate metrics; common choices are the Wasserstein metric for distributional spaces, the Riemannian metric on spheres for compositional data and on more general manifolds for manifold-valued data, the Frobenius or power metric when representing networks through their graph Laplacians, and the L^2 metric for the case of functional data. The Frobenius and power metrics, among other metrics, are also commonly used for the space of symmetric positive-definite matrices, which may also appear as outcomes, for example when correlation structures between random vectors are outcomes of interest. Another type of potential interest is the tree spaces with the BHV metric (Billera et al., 2001). All of these are geodesic metric spaces, requiring specialized approaches for causal inference. The challenge here is that these spaces, with the exception of the Hilbert space where functional data are situated, are inherently nonlinear, i.e., one does not have available linear operations such as addition, subtraction and scalar multiplication on which most established methods rely. General approaches to address these challenges for data analysis in metric spaces are discussed in Dubey et al. (2024).

Addressing causal inference for outcomes in geodesic spaces is a recent but rapidly evolving area. Recent studies include estimators for average treatment effects (Lin et al., 2023), DID (Torous et al., 2024), SCMs (Gunsilius, 2023; Gunsilius et al., 2024), and regression discontinuity designs (Van Dijcke, 2025); all of these papers focus on the special case of distributional outcomes. Recent contributions addressing more general outcomes that can be viewed as elements of a general geodesic metric space include Kurisu et al. (2024) and Zhou et al. (2025), where in the latter a geodesic DID (GDID) approach was developed.

In this paper, we introduce a geodesic synthetic control method (GSC) designed for outcomes residing in geodesic metric spaces such as those mentioned above. The GSC framework thus accommodates a broad array of outcomes residing in geodesic metric spaces. For the special case of distributional outcomes, GSC encompasses the distributional synthetic control framework of Gunsilius (2023) when using the Wasserstein metric. However, GSC also permits the use of alternative metrics in distribution space, as long as the metric space is geodesic. This includes the Fisher-Rao metric and many other distribution metrics of interest, thereby broadening the scope of analysis even for the special case of distributional outcomes.

We introduce a causal model suitable for the GSC and establish theoretical identification results for the causal effects of interest. Specific examples of causal models satisfying our assumptions in various common geodesic metric spaces illustrate the practical applicability of the proposed methodology. Additionally, we develop an augmented GSC, motivated by the augmented SCM introduced by Ben-Michael et al. (2021) for Euclidean outcomes. This extension is non-trivial due to the absence of linear algebraic structures in geodesic metric spaces; it necessitates the use of geodesic transport maps to construct our estimators.

We further propose a geodesic synthetic difference-in-differences (GSDID) estimator, extending the SDID methodology introduced by [Arkhangelsky et al. \(2021\)](#) for Euclidean outcomes. The GSDID estimator combines desirable properties of both the proposed GSC and the GDID developed by [Zhou et al. \(2025\)](#), which exhibits a double robustness property: even if the weighting schemes from either GSC or GDID individually fail to eliminate bias, their combination within the GSDID framework provides additional robustness. Moreover, the GSDID framework subsumes both the GSC and GDID as special cases.

We illustrate the efficacy of our proposed methods through comprehensive simulation studies and three real-world applications. These applications involve the employment composition changes following the 2011 Great East Japan Earthquake, the impact of abortion liberalization policy on fertility patterns in East Germany, and the health consequences of the Soviet Union’s collapse quantified through age-at-death distributions. These examples underscore the flexibility, robustness, and practical applicability of the proposed geodesic synthetic control methodologies.

The paper is organized as follows. Section 2 provides a concise review of metric geometry and introduces several geodesic metric spaces relevant for simulations and empirical analyses. Section 3 presents the proposed GSC framework, including identification results and an extension to augmented GSC. Implementation details and simulation studies for network and symmetric positive-definite matrix outcomes are described in Section 4. Section 5 illustrates the practical applicability of GSC through two empirical examples: analyzing changes in employment composition following the 2011 Great East Japan Earthquake, and assessing the impact of abortion liberalization on fertility patterns in East Germany. Section 6 extends the methodology to GSDID, presenting identification results along with an illustrative example investigating the health consequences of the Soviet Union’s collapse through age-at-death distributions. Finally, Section 7 concludes the paper. Proofs of theoretical results are provided in the Appendix.

2. PRELIMINARIES ON METRIC GEOMETRY

We review here some essential concepts from metric geometry that are needed to study outcomes in general metric spaces (\mathcal{M}, d) . A *curve* in \mathcal{M} is a continuous map $\gamma : [0, 1] \rightarrow \mathcal{M}$, whose length is defined as

$$\ell(\gamma) = \sup \sum_{i=0}^{I-1} d(\gamma(t_i), \gamma(t_{i+1})),$$

where the supremum is taken over all possible finite partitions $0 = t_0 \leq \dots \leq t_I = 1$. A curve γ is called a *geodesic* if it satisfies $d(\gamma(s), \gamma(t)) = |t - s|d(\gamma(0), \gamma(1))$ for all $s, t \in [0, 1]$. The metric space \mathcal{M} is called a *geodesic space* if, for any two points $\alpha, \beta \in \mathcal{M}$, there exists a geodesic connecting them, denoted $\gamma_{\alpha, \beta}$. If this geodesic is unique for every pair of points in \mathcal{M} , the space is referred to as a *unique geodesic space* ([Bridson and Haefliger, 1999](#)). A basic assumption for our approach is that the outcomes reside in such a space.

Examples of unique geodesic spaces that frequently arise in applications are as follows. We will revisit some of these example spaces in our simulation studies and empirical applications.

Example 2.1 (Networks). Consider the space of simple, undirected, weighted networks with m nodes and bounded edge weights. Each network can be uniquely represented by its graph Laplacian matrix. The space of graph Laplacians \mathcal{L} serves as a natural framework for characterizing network structures ([Kolaczyk and Csárdi, 2014](#); [Severn et al., 2022](#); [Zhou and Müller, 2022](#)). When endowed with the Frobenius metric, defined as $d_F(L_1, L_2) = \|L_1 - L_2\|_F$ for $L_1, L_2 \in \mathcal{L}$, the space \mathcal{L} becomes

a unique geodesic space. In this setting, the geodesic between L_1 and L_2 is given by the linear interpolation $\gamma_{L_1, L_2}(t) = (1-t)L_1 + tL_2$ for $t \in [0, 1]$.

Example 2.2 (Compositional Data). Compositional data, represented by vectors of non-negative proportions summing to one, reside in the simplex

$$\Delta^{d-1} = \{\mathbf{y} \in \mathbb{R}^d : y_j \geq 0, \sum_{j=1}^d y_j = 1\}.$$

Adopting the square-root transformation provides a map from Δ^{d-1} to the positive orthant of the unit sphere \mathcal{S}_+^{d-1} (Scealy and Welsh, 2011), where the induced geodesic distance on \mathcal{S}_+^{d-1} is the arc-length distance

$$d_g(\mathbf{z}_1, \mathbf{z}_2) = \arccos(\mathbf{z}'_1 \mathbf{z}_2),$$

with $\mathbf{z}_1, \mathbf{z}_2 \in \mathcal{S}_+^{d-1}$. Let $\theta = \arccos(\mathbf{z}'_1 \mathbf{z}_2)$ be the angle between \mathbf{z}_1 and \mathbf{z}_2 and $\|\cdot\|$ be the standard Euclidean metric. The geodesic connecting \mathbf{z}_1 and \mathbf{z}_2 is then

$$\gamma_{\mathbf{z}_1, \mathbf{z}_2}(t) = \cos(t\theta)\mathbf{z}_1 + \sin(t\theta) \frac{\mathbf{z}_2 - (\mathbf{z}'_1 \mathbf{z}_2)\mathbf{z}_1}{\|\mathbf{z}_2 - (\mathbf{z}'_1 \mathbf{z}_2)\mathbf{z}_1\|}, \quad t \in [0, 1].$$

Example 2.3 (Symmetric Positive-Definite Matrices). The space of $m \times m$ symmetric positive-definite (SPD) matrices, denoted by Sym_m^+ , plays a crucial role in various fields such as computer vision (Cherian and Sra, 2016), signal processing (Arnaudon et al., 2013) and neuroimaging (Dryden et al., 2009). Various metrics have been introduced to endow Sym_m^+ with a meaningful geometric structure, depending on the application. The Frobenius metric d_F induces unique geodesics that are simple linear interpolations, $\gamma_{A, B}(t) = (1-t)A + tB$ for $A, B \in \text{Sym}_m^+$ and $t \in [0, 1]$. The space Sym_m^+ also forms a unique geodesic space under various other metrics such as the Log-Euclidean metric (Arsigny et al., 2007), the power metric family (Dryden et al., 2009) or the Log-Cholesky metric (Lin, 2019). For instance, when adopting the log-Euclidean metric, the unique geodesic connecting $A, B \in \text{Sym}_m^+$ is given by

$$\gamma_{A, B}(t) = \exp\{(1-t)\log A + t\log B\}, \quad t \in [0, 1],$$

where $\exp(A)$ and $\log(A)$ are the matrix exponential and logarithmic maps for a real matrix A .

Example 2.4 (One-Dimensional Probability Distributions). Let \mathcal{W} denote the space of one-dimensional probability distributions on \mathbb{R} with finite second moments, equipped with the 2-Wasserstein distance

$$d_{\mathcal{W}}(\mu, \nu) = \left(\int_0^1 \{F_\mu^{-1}(s) - F_\nu^{-1}(s)\}^2 ds \right)^{1/2},$$

where F_μ^{-1} and F_ν^{-1} are the quantile functions of the probability measures μ and ν , respectively. The Wasserstein space \mathcal{W} is a complete, separable and unique geodesic space (Ambrosio et al., 2008), with geodesics given by McCann's interpolant (McCann, 1997)

$$\gamma_{\mu, \nu}(t) = \{\text{id} + t(F_\nu^{-1} \circ F_\mu - \text{id})\}_{\#}\mu, \quad t \in [0, 1],$$

where id denotes the identity map, F_μ is the cumulative distribution function of μ , and $\tau_{\#}\mu$ denotes the pushforward measure of μ by τ .

An alternative metric that is easy to compute for both univariate and multivariate distributions and is of some practical interest is the Fisher-Rao metric

$$d_{FR}(\mu, \nu) = \arccos \left(\int_{\mathbb{R}} \sqrt{f_{\mu}(x)f_{\nu}(x)} dx \right),$$

where f_{μ} and f_{ν} are the probability density functions of the measures μ and ν , respectively.

Example 2.5 (Functional Data). In functional data analysis, one considers data consisting of functions that are considered to be the realizations of a square integrable stochastic process, usually assumed to be defined on a finite interval. Such data are common in the social, physical and life sciences (Ramsay and Silverman, 2005; Hsing and Eubank, 2015; Wang et al., 2016). Typically, functional data are assumed to be situated in the Hilbert space $L^2(\mathcal{T})$ of square integrable functions, where \mathcal{T} is a compact interval, most commonly a time domain. In contrast to the other metric spaces we consider in this paper, this space is a vector space and thus permits algebraic operations. It is equipped with the standard L^2 metric

$$d_{L^2}(g_1, g_2) = \left(\int_{\mathcal{T}} \{g_1(t) - g_2(t)\}^2 dt \right)^{1/2}, \quad g_1, g_2 \in L^2(\mathcal{T}),$$

making $L^2(\mathcal{T})$ a unique geodesic space, with the unique geodesic between g_1 and g_2 given by

$$\gamma_{g_1, g_2}(t) = (1 - t)g_1 + tg_2, \quad t \in [0, 1].$$

3. GEODESIC SYNTHETIC CONTROL METHODS

3.1. Construction of the estimator. Consider a standard panel data setting for the synthetic control method (SCM), where outcomes are observed for $J+1$ units over T time periods, indexed by $j = 1, \dots, J+1$ and $t = 1, \dots, T$, respectively. In what follows, we fix both J and T . For Euclidean outcomes $Y_{j,t} \in \mathbb{R}^q$, the conventional SCM is as follows. Assume that for a time $T_0 > 1$ only the unit indexed by $j = 1$ experienced the intervention at times t with $T_0 < t \leq T$. We denote the potential outcomes of unit j at time t with and without intervention by $Y_{j,t}(I)$ and $Y_{j,t}(N)$, respectively. We observe $Y_{j,t} = Y_{j,t}(I)$ only for $j = 1$ and $t = T_0 + 1, \dots, T$. For all other combinations of j and t we observe $Y_{j,t} = Y_{j,t}(N)$. The causal effect of interest is $\tau_t = Y_{1,t}(I) - Y_{1,t}(N) = Y_{1,t} - Y_{1,t}(N)$ for $t = T_0 + 1, \dots, T$. The SCM is a method to predict $Y_{1,t}(N)$ for $t = T_0 + 1, \dots, T$ using the control units $\{Y_{j,t} = Y_{j,t}(N)\}_{2 \leq j \leq J+1, 1 \leq t \leq T}$.

In the SCM, the predicted value for $Y_{1,t}(N)$ is constructed as

$$Y_{1,t}^{(SC)} := \sum_{j=2}^{J+1} \bar{w}_j Y_{j,t} = \arg \min_{y \in \mathbb{R}^q} \sum_{j=2}^{J+1} \bar{w}_j \|y - Y_{j,t}\|^2, \quad t = T_0 + 1, \dots, T,$$

where the weights are given by

$$\begin{aligned} \bar{\mathbf{w}} &= (\bar{w}_2, \dots, \bar{w}_{J+1})' \in \arg \min_{\mathbf{w} \in \Delta^{J-1}} \frac{1}{T_0} \sum_{t=1}^{T_0} \left\| Y_{1,t} - Y_{2:J+1,t}^{(\mathbf{w})} \right\|^2, \\ Y_{2:J+1,t}^{(\mathbf{w})} &= \sum_{j=2}^{J+1} w_j Y_{j,t} = \arg \min_{y \in \mathbb{R}^q} \sum_{j=2}^{J+1} w_j \|y - Y_{j,t}\|^2, \\ \Delta^{J-1} &= \{ \mathbf{w} = (w_2, \dots, w_{J+1})' \in \mathbb{R}^J : w_j \geq 0, \sum_{j=2}^{J+1} w_j = 1 \}, \end{aligned}$$

and thus are based only on the observations made at times t with $1 \leq t \leq T_0$. This motivates to obtain the estimate of the causal effect τ_t as $\tau_t^{(\text{SC})} = Y_{1,t} - Y_{1,t}^{(\text{SC})}$. The estimators $\{\tau_t^{(\text{SC})}\}_{t=T_0+1, \dots, T}$ are referred to synthetic control estimators.

To extend the SCM for outcomes residing in a unique geodesic space (\mathcal{M}, d) one needs to substitute the algebraic operation of taking a difference that is crucial for the definition of the estimator $\tau_t^{(\text{SC})}$, since one cannot take sums or differences of random objects in general metric spaces. Here, the assumption that the underlying space is geodesic becomes essential. In Euclidean spaces, the difference $\beta - \alpha$ can be equivalently interpreted as movement along the geodesic (straight line) connecting α to β . This insight motivates the generalization of differences to geodesics connecting corresponding points (Kurisu et al., 2024). Accordingly, we introduce the causal effect of the intervention in a unique geodesic space as the geodesic from $Y_{1,t}(N)$ to $Y_{1,t}(I)$, i.e.,

$$\tau_t = \gamma_{Y_{1,t}(N), Y_{1,t}(I)}, \quad t = T_0 + 1, \dots, T. \quad (3.1)$$

To provide additional motivation why this makes sense, in the Euclidean (vector) case the difference $Y_{1,t}(I) - Y_{1,t}(N)$ utilizes both the shortest distance and directional information when moving from $Y_{1,t}(N)$ to $Y_{1,t}(I)$. Since a geodesic connecting points α and β in a geodesic metric space (\mathcal{M}, d) embodies both the shortest distance and directional information from α to β with respect to the metric d , τ_t emerges as a natural extension of quantifying treatment effects in geodesic metric spaces.

To estimate the causal effect τ_t in (3.1), we adopt a natural extension of the construction of synthetic weights in the Euclidean case and then obtain the predicted value for $Y_{1,t}(N)$ as $Y_{1,t}^{(\text{GSC})} = \arg \min_{\nu \in \mathcal{M}} \sum_{j=2}^{J+1} \bar{w}_j d^2(\nu, Y_{j,t})$, where

$$\begin{aligned} \bar{\mathbf{w}} &\in \arg \min_{\mathbf{w} \in \Delta^{J-1}} \frac{1}{T_0} \sum_{t=1}^{T_0} d^2(Y_{1,t}, Y_{2:J+1,t}^{(\mathbf{w})}), \\ Y_{2:J+1,t}^{(\mathbf{w})} &= \arg \min_{\nu \in \mathcal{M}} \sum_{j=2}^{J+1} w_j d^2(\nu, Y_{j,t}). \end{aligned} \quad (3.2)$$

The resulting geodesic synthetic control (GSC) estimator in unique geodesic spaces is

$$\tau_t^{(\text{GSC})} := \gamma_{Y_{1,t}^{(\text{GSC})}, Y_{1,t}}, \quad t = T_0 + 1, \dots, T.$$

A key step for the generalization of the SCM to the case of outcomes residing in geodesic metric spaces is the construction of the weight vector $\bar{\mathbf{w}}$ in (3.2) by adopting a metric version of the weighted average $Y_{2:J+1,t}^{(\mathbf{w})}$ that corresponds to a weighted Fréchet mean or barycenter (Fréchet, 1948; Ginestet et al., 2012). Theoretical justifications are provided in the next subsection.

3.2. Causal model for the geodesic synthetic control method. Consider the following model for potential outcomes without intervention:

$$Y_{j,t}(N) = g_t(U_j), \quad t = 1, \dots, T, \quad j = 1, \dots, J + 1, \quad (3.3)$$

where $U_j \in \mathcal{M}$ is an unobservable time-invariant characteristic of unit j and $g_t(\cdot) : \mathcal{M} \rightarrow \mathcal{M}$ is a measurable function defined on the metric space \mathcal{M} . Figure 1 illustrates the causal framework for GSC with metric space-valued (random object) outcomes.

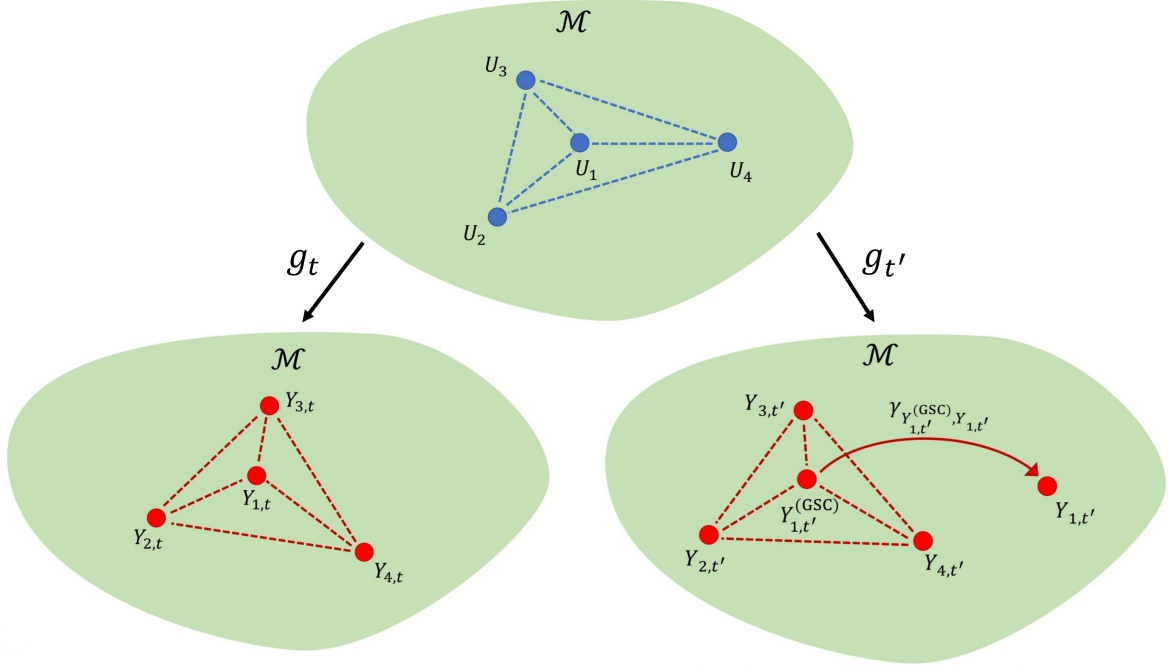


FIGURE 1. Illustration of the causal framework for the geodesic synthetic control method when $t \leq T_0$ and $t' \geq T_0 + 1$. The circles symbolize random objects located in the geodesic metric space \mathcal{M} . The solid red arrow in the right lower subfigure represents the geodesic path from $Y_{1,t'}^{(\text{GSC})}$ to $Y_{1,t'}$ that corresponds to the geodesic synthetic control estimator.

Define

$$g_t^{(\mathbf{w})}(U_{2:J+1}) = \arg \min_{\nu \in \mathcal{M}} \sum_{j=2}^{J+1} w_j d^2(\nu, g_t(U_j)), \quad \mathbf{w} \in \Delta^{J-1},$$

$$\mathbb{W}_t^* = \{\mathbf{w} \in \Delta^{J-1} : d(g_t(U_1), g_t^{(\mathbf{w})}(U_{2:J+1})) = 0\}, \quad t = 1, \dots, T.$$

We impose the following assumptions.

Assumption 3.1.

- (i) For each $\mathbf{w} \in \Delta^{J-1}$ and $t = 1, \dots, T$, $g_t^{(\mathbf{w})}(U_{2:J+1})$ uniquely exists.
- (ii) $\bigcap_{t=1}^{T_0} \mathbb{W}_t^*$ is not empty and $\bigcap_{t=1}^{T_0} \mathbb{W}_t^* \subset \bigcap_{t=T_0+1}^T \mathbb{W}_t^*$.

Assumption 3.1 (ii) ensures the existence of a non-empty subset $\bigcap_{t=1}^{T_0} \mathbb{W}_t^*$ within Δ^{J-1} such that for any $\mathbf{w} \in \bigcap_{t=1}^{T_0} \mathbb{W}_t^*$ the condition $d(g_t(U_1), g_t^{(\mathbf{w})}(U_{2:J+1})) = 0$ holds for all $t = 1, \dots, T$. This is the natural generalization of the perfect pretreatment fit assumption from equation (2) in Abadie et al. (2010) to the unique geodesic space setting that we consider here.

Assumption 3.1 can be verified in models of the form $g_t(U_j) = \gamma_{\mu_t, U_j}(\alpha_t)$ with $\mu_t \in \mathcal{M}$ and $\alpha_t \in (0, 1)$ in spaces such as networks (Example 2.1), Wasserstein space (Example 2.4), functional data (Example 2.5) as well as SPD matrices (Example 2.3) when the latter are equipped with the Frobenius metric, the power metric family, the Log-Euclidean metric or the Log-Cholesky metric. For the space of compositional data \mathcal{S}_+^{d-1} as discussed in Example 2.2, Assumption 3.1 can be

verified for the model $g_t(U_j) = \text{Exp}_{\mu_t}(A_t \text{Log}_{U_1}(U_j))$, where A_t is a $(d-1) \times (d-1)$ positive-definite matrix and Exp_{μ} and Log_{μ} are the Riemannian exponential and logarithmic maps at $\mu \in \mathcal{M}$, respectively. Details on verifying the assumption for these special cases are in Appendix A.

In the special case where the metric space (\mathcal{M}, d) corresponds to the Euclidean space $(\mathbb{R}^q, \|\cdot\|)$ with the standard Euclidean norm, geodesics are straight lines and the causal model $g_t(U_j) = \gamma_{\mu_t, U_j}(\alpha_t)$ simplifies to $g_t(U_j) = \mu_t + \alpha_t(U_j - \mu_t)$, which corresponds to a linear factor model without covariates and error terms. For the case where covariates are available, we introduce an augmented version in Section 3.3 to address potential biases in the GSC that may arise due to imperfect pretreatment fit.

The following result establishes model identification of the GSC.

Theorem 3.1. *Suppose that Assumption 3.1 holds for model (3.3). Then $Y_{1,t}^{(\text{GSC})} = Y_{1,t}(N)$ for each $t = T_0 + 1, \dots, T$.*

It is possible to extend model (3.3) to the case where the unobservable characteristics vary over time, i.e., $Y_{j,t}(N) = g_t(U_{j,t})$ for $t = 1, \dots, T$, $j = 1, \dots, J+1$, where $U_{j,t} \in \mathcal{M}$ is an unobservable characteristic of unit j that may change over time t . In this scenario, result similar to Theorem 3.1 holds if we additionally assume that the set $\mathbf{W}_t^* = \{\mathbf{w} \in \Delta^{J-1} : d^2(g_t(U_{1,t}), g_t^{(\mathbf{w})}(U_{2:J+1,t})) = 0\}$ satisfies a slightly modified version of Assumption 3.1 (ii).

Remark 3.1 (*Geodesic synthetic control method with negative weights*). Instead of weight vectors situated in the simplex Δ^{J-1} in (3.2), one could also use more general weights

$$\Sigma^{J-1} = \{\mathbf{w} = (w_2, \dots, w_{J+1})' \in \mathbb{R}^J : \sum_{j=2}^{J+1} w_j = 1\}$$

that may include negative elements. If such more general weight vectors satisfy a condition similar to Assumption 3.1 (ii), the results will remain unchanged, however the GSC with possibly negative weights may overfit the pre-treatment data. To improve out-of-sample performance, one possible approach is to select weights by minimizing a penalized objective function, as considered in Arkhangelsky et al. (2021).

Remark 3.2 (*Geodesic synthetic control method with covariates*). Suppose covariates $\{X_{j,t} \in (\mathcal{M}_X, d_X) : j = 1, \dots, J+1, t = 1, \dots, T\}$ are available, where the metric space (\mathcal{M}_X, d_X) in general will differ from the outcome space (\mathcal{M}, d) and often will correspond to the Euclidean space \mathbb{R}^q for a $q \geq 1$. One can then modify the dependence of the GSC weights on the covariates as follows,

$$\tau_t^{(\text{COV})} := \gamma_{Y_{1,t}^{(\text{COV})}, Y_{1,t}}, \quad t = T_0 + 1, \dots, T,$$

where

$$Y_{1,t}^{(\text{COV})} = \arg \min_{\nu \in \mathcal{M}} \sum_{j=2}^{J+1} \bar{w}_j(X) d^2(\nu, Y_{j,t}),$$

$$\bar{\mathbf{w}}(X) = (\bar{w}_2(X), \dots, \bar{w}_{J+1}(X))' \in \arg \min_{\mathbf{w} \in \Delta^{J-1}} \frac{1}{T_0} \sum_{t=1}^{T_0} d_X^2(X_{1,t}, X_{2:J+1,t}^{(\mathbf{w})}),$$

$$X_{2:J+1,t}^{(\mathbf{w})} = \arg \min_{\nu \in \mathcal{M}} \sum_{j=2}^{J+1} w_j d_X^2(\nu, X_{j,t}), \quad \mathbf{w} \in \Delta^{J-1}.$$

Adopting the metric $d_X^2 := d_1^2 + \dots + d_k^2$ for the space $\mathcal{M}_X := \mathcal{M}_1 \times \dots \times \mathcal{M}_k$, one can also consider multiple covariates $X_{j,t} = (X_{j,t}^{(1)}, \dots, X_{j,t}^{(k)}) \in (\mathcal{M}_1, d_1) \times \dots \times (\mathcal{M}_k, d_k)$. This would provide an extension of the approach of [Abadie et al. \(2010\)](#), who discuss the use of covariates for weight selection in the implementation of the SCM for Euclidean outcomes.

Remark 3.3 (*Placebo permutation test*). In order to formally test for the presence of a causal effect, one may employ a placebo permutation test ([Abadie, 2021](#)). In addition to the synthetic control predicted value $Y_{1,t}^{(\text{GSC})}$, we compute $Y_{j,t}^{(\text{GSC})}$ for $j = 2, \dots, J+1$ by applying the same algorithm as used to obtain $Y_{1,t}^{(\text{GSC})}$, pretending the treatment unit is j . If there is an actual treatment effect only in unit $j = 1$, then the distance $d(Y_{1,t}, Y_{1,t}^{(\text{GSC})})$ for the actual treatment unit should be among the most extreme in $\{d(Y_{j,t}, Y_{j,t}^{(\text{GSC})}) : j = 1, \dots, J+1\}$. In this framework, the p -value for testing the null hypothesis of no causal effect by the intervention to unit $j = 1$ is

$$\frac{\text{rank of } d(Y_{1,t}, Y_{1,t}^{(\text{GSC})}) \text{ in } \{d(Y_{j,t}, Y_{j,t}^{(\text{GSC})}) : j = 1, \dots, J+1\}}{J+1}, \quad t = T_0 + 1, \dots, T.$$

3.3. Augmented geodesic synthetic control method. In some applications, $Y_{1,t}(N)$ may not be in the convex hull of control units $\{Y_{2,t}, \dots, Y_{J+1,t}\}$ implying that $Y_{1,t}(N) \neq Y_{2:J+1,t}^{(\mathbf{w})}$ for any $\mathbf{w} \in \Delta^{J-1}$. In this case, the GSC estimator will be biased for the true causal effect τ_t . To address this issue, we propose the augmented GSC, which is a regression-adjusted version of the GSC ([Ben-Michael et al., 2021](#)). The augmented GSC aims to reduce the bias of the GSC when covariates are available. If covariates are not available, one can instead use the geodesic synthetic difference-in-differences discussed in Section 6 below, which addresses the bias of the GSC by taking weighted averages not only over units but also over timepoints.

To construct the augmented GSC estimator, we introduce the notion of geodesic transport maps, with concrete examples provided in [Remark 3.5](#) below.

Assumption 3.2. *Let (\mathcal{M}, d) be a unique geodesic space. For any two points $\alpha, \beta \in \mathcal{M}$, there exists a geodesic transport map $\Gamma_{\alpha,\beta} : \mathcal{M} \rightarrow \mathcal{M}$ satisfying $\Gamma_{\alpha,\beta}(\alpha) = \beta$ and for any $\omega \in \mathcal{M}$, there exists a unique point $\zeta \in \mathcal{M}$ such that $\Gamma_{\alpha,\beta}(\omega) = \zeta$.*

This assumption ensures that the geodesic joining points α and β can be naturally extended from any other point $\omega \in \mathcal{M}$, yielding a uniquely defined endpoint $\zeta \in \mathcal{M}$. In Euclidean space \mathbb{R}^q , the transport map is explicitly defined as $\Gamma_{\alpha,\beta}(\omega) = \omega + (\beta - \alpha)$, and this definition extends naturally to general vector spaces, where geodesics correspond to vector translations, as well as to Riemannian manifolds via parallel transport ([Yuan et al., 2012](#); [Lin and Yao, 2019](#); [Chen et al., 2023a](#)). Such geodesic transport maps exist widely in metric spaces encountered in practical applications ([Zhu and Müller, 2023](#)); see [Remark 3.5](#) for further details.

Consider a metric space (\mathcal{M}_X, d_X) that may differ from (\mathcal{M}, d) and the corresponding data pairs $\{(Y_{j,1:T}, \mathbf{X}_{j,1:T_0})\}_{1 \leq j \leq J+1}$, where $\mathbf{Y}_{j,1:s} = (Y_{j,1}, \dots, Y_{j,s}) \in \mathcal{M}^s$ and $\mathbf{X}_{j,1:s} = (X_{j,1}, \dots, X_{j,s}) \in \mathcal{M}_X^s$. Denote by $m_t(\mathbf{Z}_{j,1:T_0})$ a regression model aiming to predict $Y_{j,t}(N)$ for $t = T_0 + 1, \dots, T$, where $\mathbf{Z}_{j,1:T_0} = (\mathbf{Y}_{j,1:T_0}, \mathbf{X}_{j,1:T_0})$ and let $\hat{m}_t(\cdot)$ be its estimated version using data $\{(Y_{j,t}, \mathbf{Z}_{j,1:T_0})\}_{2 \leq j \leq J+1}$. Define

$$m_t^{(\bar{\mathbf{w}})}(\mathbf{Z}_{2:J+1,1:T_0}) = \arg \min_{\nu \in \mathcal{M}} \sum_{j=2}^{J+1} \bar{w}_j d^2(\nu, m_t(\mathbf{Z}_{j,1:T_0})),$$

where $\bar{\omega} \in \Delta^{J-1}$ is an optimal weight vector. Then the augmented GSC estimator is

$$\tau_t^{(\text{AGSC})} := \gamma_{Y_{1,t}^{(\text{AGSC})}, Y_{1,t}}, \quad t = T_0 + 1, \dots, T,$$

where

$$Y_{1,t}^{(\text{AGSC})} = \Gamma_{\hat{m}_t^{(\bar{\omega})}(\mathbf{Z}_{2:J+1,1:T_0}), \hat{m}_t(\mathbf{Z}_{1,1:T_0})}(Y_{1,t}^{(\text{GSC})}).$$

To see the rationale for this estimator, denote by $\mathcal{G}(\mathcal{M}) = \{\gamma_{\alpha,\beta} : \alpha, \beta \in \mathcal{M}\}$ the space of geodesics of the unique geodesic space \mathcal{M} . To compare geodesics, we define a binary relation \sim on $\mathcal{G}(\mathcal{M})$ through the geodesic transport map, where $\gamma_{\alpha_1,\beta_1} \sim \gamma_{\alpha_2,\beta_2}$ if and only if $\Gamma_{\alpha_1,\beta_1}(\omega) = \Gamma_{\alpha_2,\beta_2}(\omega)$ for all $\omega \in \mathcal{M}$. Indeed the binary relation \sim is an equivalence relation on $\mathcal{G}(\mathcal{M})$ (Zhou et al., 2025). If the geodesic $\gamma_{\hat{m}_t^{(\bar{\omega})}(\mathbf{Z}_{2:J+1,1:T_0}), \hat{m}_t(\mathbf{Z}_{1,1:T_0})}$ serves as a substitute for the bias of the GSC estimator, the following result justifies the augmented GSC.

Proposition 3.1. *Under Assumption 3.2, suppose $\gamma_{\hat{m}_t^{(\bar{\omega})}(\mathbf{Z}_{2:J+1,1:T_0}), \hat{m}_t(\mathbf{Z}_{1,1:T_0})} \sim \gamma_{Y_{1,t}^{(\text{GSC})}, Y_{1,t}(N)}$ for $t = T_0 + 1, \dots, T$. Then*

$$Y_{1,t}(N) = \Gamma_{\hat{m}_t^{(\bar{\omega})}(\mathbf{Z}_{2:J+1,1:T_0}), \hat{m}_t(\mathbf{Z}_{1,1:T_0})}(Y_{1,t}^{(\text{GSC})}), \quad t = T_0 + 1, \dots, T.$$

Figure 2 illustrates the augmented GSC. For Euclidean outcomes, the augmented GSC estimator can be represented as

$$Y_{1,t}^{(\text{AGSC})} = \underbrace{\sum_{j=2}^{J+1} \bar{w}_j Y_{j,t}}_{=Y_{1,t}^{(\text{GSC})}} + \overbrace{\hat{m}_t(\mathbf{Z}_{1,1:T_0}) - \sum_{j=2}^{J+1} \bar{w}_j \hat{m}_t(\mathbf{Z}_{j,1:T_0})}^{\text{bias correction}} = \hat{m}_t(\mathbf{Z}_{1,1:T_0}) + \sum_{j=2}^{J+1} \bar{w}_j (Y_{j,t} - \hat{m}_t(\mathbf{Z}_{j,1:T_0})),$$

$= \hat{m}_t^{(\bar{\omega})}(\mathbf{Z}_{2:J+1,1:T_0})$

which coincides with the augmented SC estimator of Ben-Michael et al. (2021). Hence, the proposed augmented GSC estimator $Y_{1,t}^{(\text{AGSC})}$ is a natural extension of the conventional augmented synthetic control estimator.

Remark 3.4 (Regression estimator). To implement the augmented GSC with $X_{j,t} \in \mathcal{M}$, one can use the geodesic optimal transport regression (Zhu and Müller, 2023) to model $m_t(\mathbf{Z}_{j,1:T_0})$. For the special case where the covariates are Euclidean with $X_{j,t} \in \mathbb{R}^q$, employing global Fréchet regression (Petersen and Müller, 2019) is an option to implement $m_t(\mathbf{Z}_{j,1:T_0}) = m_t(\mathbf{X}_{j,1:T_0})$ in order to predict $Y_{j,t}(N)$ for $t = T_0 + 1, \dots, T$, as follows:

$$\hat{m}_t(\mathbf{x}) = \arg \min_{\nu \in \mathcal{M}} \frac{1}{J} \sum_{j=2}^{J+1} \{1 + (\mathbf{X}_{j,1:T_0} - \bar{\mathbf{X}}_{1:T_0})' \hat{\Sigma}_{1:T_0}^{-1} (\mathbf{x} - \bar{\mathbf{X}}_{1:T_0})\} d^2(\nu, Y_{j,t}),$$

where $\mathbf{X}_{j,1:T_0} = (X'_{j,1}, \dots, X'_{j,T_0})'$,

$$\bar{\mathbf{X}}_{1:T_0} = \frac{1}{J} \sum_{j=2}^{J+1} \mathbf{X}_{j,1:T_0}, \quad \hat{\Sigma}_{1:T_0} = \frac{1}{J} \sum_{j=2}^{J+1} (\mathbf{X}_{j,1:T_0} - \bar{\mathbf{X}}_{1:T_0})(\mathbf{X}_{j,1:T_0} - \bar{\mathbf{X}}_{1:T_0})'.$$

Remark 3.5 (Examples of geodesic transport maps). We provide here specific geodesic transport maps that satisfy Assumption 3.2 for Examples 2.1–2.5 in Section 2. For the space of networks in Example 2.1, the geodesic corresponds to the line segment connecting the start and end points. Then the geodesic transport map is given as $\Gamma_{\alpha,\beta}(\omega) = \omega + (\beta - \alpha)$.

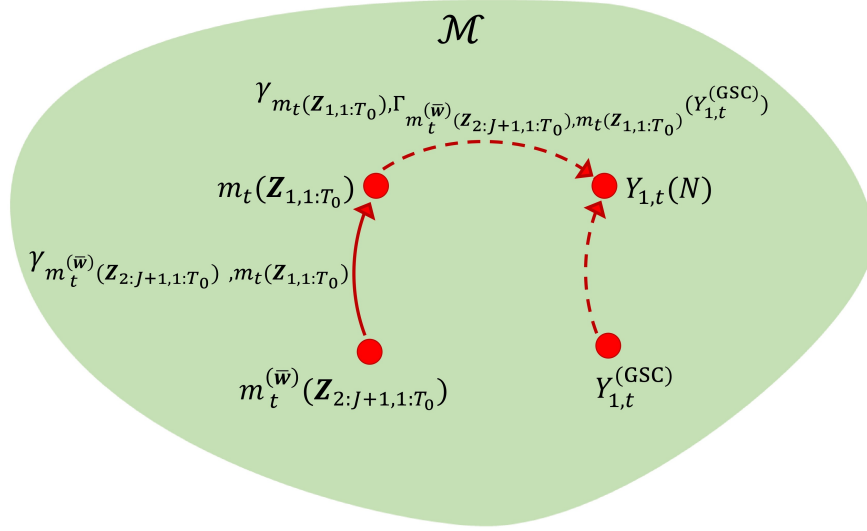


FIGURE 2. Illustration of the augmented geodesic synthetic control method. The circles symbolize random objects in the geodesic metric space \mathcal{M} and the arrows depict geodesics that connect the objects. The geodesic corresponding to the dashed red arrow from $Y_{1,t}^{(\text{GSC})}$ to $Y_{1,t}(N)$ represents the bias of the geodesic synthetic control method in the setting considered in Section 3.3. The solid red arrow represents the geodesic connecting $m_t^{(\bar{w})}(\mathbf{Z}_{2:J+1,1:T_0})$ and $m_t(\mathbf{Z}_{1,1:T_0})$ that serves as a substitute to assess the bias of the geodesic synthetic control estimator. The dashed red arrow from $m_t(\mathbf{Z}_{1,1:T_0})$ to $Y_{1,t}(N)$ represents the bias correction for the geodesic synthetic control estimator corresponding to the augmented geodesic control estimator.

For the space of compositional data in Example 2.2, the geodesic transport map can be interpreted as a rotation of the point ω along the geodesic determined by α and β . The tangent vector for the geodesic $\gamma_{\alpha,\beta}$ is given by $v_{\alpha,\beta} = \beta - (\alpha'\beta)\alpha$, whose magnitude and direction encode the geodesic length and directionality needed to move from α to β along the sphere. The geodesic transport map is then defined as $\Gamma_{\alpha,\beta}(\omega) = \text{Exp}_\omega(\theta_{\alpha,\beta}v/\|v\|)$, where $\theta_{\alpha,\beta}$ is the angle between α and β , and $v = v_{\alpha,\beta} - (\omega'v_{\alpha,\beta})\omega$ is the projection of $v_{\alpha,\beta}$ onto the tangent space at ω .

For the space of SPD matrices in Example 2.3, the geodesic transport map induced by the Frobenius metric is the line segment connecting two points. Then the geodesic transport map is $\Gamma_{\alpha,\beta}(\omega) = \omega + (\beta - \alpha)$. The geodesic transport map induced by the Log-Euclidean metric is $\Gamma_{\alpha,\beta}(\omega) = \exp\{\log \omega + (\log \beta - \log \alpha)\}$ and for the power metric family it is $\Gamma_{\alpha,\beta}(\omega) = [\omega^p + (\beta^p - \alpha^p)]^{1/p}$ where $p > 0$ is a constant denoting the power, $A^p = U\Lambda^pU'$ and $U\Lambda U'$ is the usual spectral decomposition of $A \in \text{Sym}_m^+$. Let \mathcal{L}_m^+ be the set of lower triangular matrices with positive diagonal entries. For any $S \in \text{Sym}_m^+$, there exists a unique $L \in \mathcal{L}_m^+$ such that $S = LL'$ and a diffeomorphism \mathcal{L} between Sym_m^+ and \mathcal{L}_m^+ . For any $L \in \mathcal{L}_m^+$, let $[L]$ be the strictly lower triangular part and $\mathbb{D}(L)$ the diagonal part of L . For $\alpha, \beta, \omega \in \mathcal{L}_m^+$, the geodesic transport map induced by the Log-Cholesky metric is $\Gamma_{\alpha,\beta}(\omega) = [\omega] + ([\beta] - [\alpha]) + \exp\{\log(\mathbb{D}(\omega)) + (\log(\mathbb{D}(\beta)) - \log(\mathbb{D}(\alpha)))\}$.

For the Wasserstein space in Example 2.4, the geodesic transport map is $\Gamma_{\alpha,\beta} = F_\beta^{-1} \circ F_\alpha$, where F_α and F_β^{-1} are the cumulative distribution function of the measure α and the quantile function of

the measure β , respectively. The resulting endpoint of the geodesic $\gamma_{\omega,\zeta}$ is then $F_\zeta^{-1} = F_\beta^{-1} \circ F_\alpha \circ F_\omega^{-1}$ where F_ω^{-1} and F_ζ^{-1} denote the quantile functions of the measures ω and ζ .

For the space of functional data in Example 2.5, the geodesic transport map induced by the L^2 metric is the line segment connecting two points. Then the geodesic transport map is $\Gamma_{\alpha,\beta}(\omega) = \omega + (\beta - \alpha)$.

4. IMPLEMENTATION AND SIMULATIONS

4.1. Implementation details. Algorithm 1 outlines the implementation steps for the proposed geodesic synthetic control method. The optimization problem in Step 1 of Algorithm 1 requires customized approaches that depend on the specific metric and geometry of the underlying metric space. For networks (Example 2.1), symmetric positive-definite matrices (Example 2.3), distributions (Example 2.4), and functions (Example 2.5), the optimization reduces to a straightforward convex quadratic optimization problem that can be easily implemented (Stellato et al., 2020).

For the case of compositional data (Example 2.2), the optimization becomes more challenging, as it involves minimizing a bilevel objective where the weighted Fréchet mean $Y_{2:J+1,t}^{(\mathbf{w})}$ is itself an argmin problem. Due to the complexity of analytical differentiation when nonlinear Fréchet means are involved, we adopt a derivative-free constrained optimization strategy. Specifically, we use the Constrained Optimization BY Linear Approximations (COBYLA) algorithm (Powell, 1994), as implemented in the R package `nloptr` (Johnson, 2008). The weighted Fréchet mean involved in the objective function is obtained using the R package `manifold` (Dai et al., 2021).

Algorithm 1: Geodesic Synthetic Control Method

Input: data $\{Y_{j,t} : j = 1, \dots, J + 1, t = 1, \dots, T\}$.

Output: geodesic synthetic control estimator $\tau_t^{(\text{GSC})}$ for $t = T_0 + 1, \dots, T$.

1 $\bar{\mathbf{w}} = (\bar{w}_2, \dots, \bar{w}_{J+1}) \leftarrow$ the estimated synthetic control weights:

$$\bar{\mathbf{w}} \in \arg \min_{\mathbf{w} \in \Delta^{J-1}} \frac{1}{T_0} \sum_{t=1}^{T_0} d^2(Y_{1,t}, Y_{2:J+1,t}^{(\mathbf{w})})$$

where $Y_{2:J+1,t}^{(\mathbf{w})} = \arg \min_{\nu \in \mathcal{M}} \sum_{j=2}^{J+1} w_j d^2(\nu, Y_{j,t})$ for $t = 1, \dots, T_0$;

2 $Y_{1,t}^{(\text{GSC})} = \arg \min_{\nu \in \mathcal{M}} \sum_{j=2}^{J+1} \bar{w}_j d^2(\nu, Y_{j,t}) \leftarrow$ the synthetic control unit;

3 $\tau_t^{(\text{GSC})} = \gamma_{Y_{1,t}^{(\text{GSC})}, Y_{1,t}} \leftarrow$ the geodesic synthetic control estimator.

4.2. Simulations for networks and symmetric positive-definite matrices. We conduct simulations to assess the performance of the proposed geodesic synthetic control method using networks and SPD matrices. Potential outcomes without intervention are generated via the geodesic model $Y_{j,t}(N) = \gamma_{\mu_t, U_j}(\alpha_t)$, where $\mu_t, U_j \in \mathcal{M}$ represent the deterministic time trend and the unit-specific latent characteristic, respectively. We consider a total of $T = 20$ time periods, where the treatment occurs at $T_0 = 19$, and $J = 20$ control units. The primary goal of these simulations is to evaluate how accurately the synthetic control estimator $Y_{1,T}^{(\text{GSC})}$ replicates the true counterfactual $Y_{1,T}(N)$ for the treated unit at time T .

For the network outcomes, we use graph Laplacians residing in the space \mathcal{L} equipped with the Frobenius metric (see Example 2.1). Networks are simulated via a weighted stochastic block model

with 10 nodes divided into two equal-sized communities. Edges within and between communities are generated using Bernoulli distributions with probabilities specified by the edge probability matrix $\begin{pmatrix} 0.75 & 0.1 \\ 0.1 & 0.75 \end{pmatrix}$. The weights of existing edges are generated as $\sin(0.1\pi t) + e^{-0.1t}((0.1j - 0.5)^2 - \sin(0.1\pi t))$. The graph Laplacian associated with each network is then considered to be the outcome.

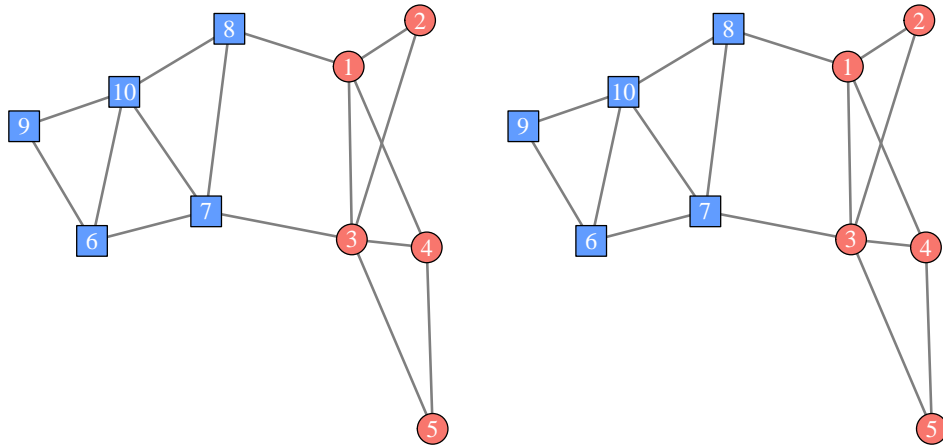
For outcomes in the space of SPD matrices Sym_m^+ equipped with the Log-Euclidean metric (see Example 2.3), we generate the underlying SPD matrices μ and U from a Wishart distribution with 12 degrees of freedom and a scale matrix of $0.1\mathbf{I}_{10}$, where \mathbf{I}_{10} denotes the 10×10 identity matrix. The deterministic time trend and the unit-specific latent characteristic are constructed as $\mu_t = 0.1t\mu$ and $U_j = e^{(0.1j-0.5)^2}U$, respectively. The parameter α_t governing the geodesic interpolation is set to $\alpha_t = \log(0.1(t + 1))$.

The counterfactual outcome for the treated unit had it not received the treatment $Y_{1,T}(N)$ and the synthetic control unit $Y_{1,T}^{(\text{GSC})}$ for networks and SPD matrices are illustrated in Figure 3. The synthetic control outcome precisely matches the true counterfactual outcome in both scenarios, highlighting the effectiveness of the GSC approach for outcomes located in complex geodesic metric spaces. These simulation results further validate the model identification established in Theorem 3.1.

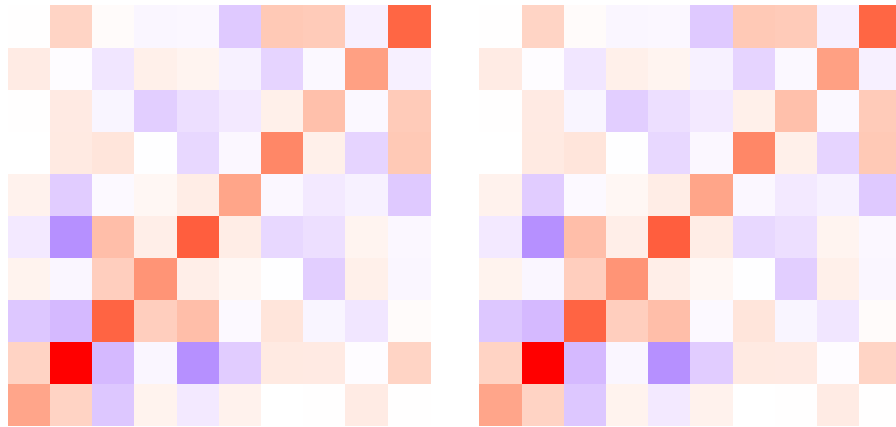
5. REAL DATA EXAMPLE

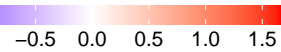
5.1. Impact of the 2011 Great East Japan Earthquake on Employment-Population Ratio by Industry. We analyze the impact of the 2011 Great East Japan Earthquake on the employment-population ratio by employment category, using data from the Research Institute of Economy, Trade and Industry (RIETI) database (<https://www.rieti.go.jp/jp/database/R-JIP2021/index.html>). These data provide annual employment figures by industry for each prefecture in Japan from 1994 to 2018. Employment is categorized into three broad groups: primary (agriculture, forestry, and fisheries), secondary (manufacturing, electricity, gas, water supply, waste management and construction) and tertiary (services, including wholesale/retail, finance, and healthcare). For each prefecture and each year, the employment shares (proportions) across these three categories are represented as a three-dimensional compositional vector. The component-wise square root transformation (see Example 2.2) maps these compositional outcomes onto the positive quadrant of the sphere $\mathcal{S}_+^2 \subset \mathbb{R}^3$, which we endow with the geodesic metric. Unlike standard synthetic control approaches that typically analyze each compositional component separately, the proposed approach considers the entire compositional vector jointly. This holistic perspective reflects the intrinsic geometry of compositional data, thereby capturing interdependencies of employment across the three categories.

The Great East Japan Earthquake occurred on March 11, 2011, causing widespread devastation, particularly in Miyagi Prefecture, which suffered the highest number of fatalities. The earthquake significantly disrupted economic activity, leading to structural shifts in employment. To assess the impact of the earthquake on employment composition, we define Miyagi Prefecture as the treated unit, while control units are selected from prefectures located on Japan’s main island with a population between 1 million and 4 million in 2010, excluding the heavily affected areas of Fukushima, Iwate, and Miyagi. This results in a control group consisting of 19 prefectures: Akita, Gifu, Gunma, Hiroshima, Ibaraki, Ishikawa, Kyoto, Mie, Nagano, Nara, Niigata, Okayama,



(A)



value  -0.5 0.0 0.5 1.0 1.5

(B)

FIGURE 3. Simulated counterfactual outcome for the treated unit had it not received the treatment $Y_{1,T}(N)$ (left) and the corresponding synthetic control outcome $Y_{1,T}^{(GSC)}$ (right) using the proposed method for (A) networks and (B) SPD matrices. For networks, nodes from the two communities are represented by red circles and blue squares, respectively. For SPD matrices, outcomes are visualized as heatmaps.

Shiga, Shizuoka, Tochigi, Toyama, Wakayama, Yamagata and Yamaguchi. The analysis considers the period 2008–2010 as pre-treatment and 2011–2013 as post-treatment to capture the immediate effects of the earthquake on employment composition.

We apply the proposed GSC to estimate the causal effect of the earthquake. The method constructs a synthetic counterpart for Miyagi Prefecture as a weighted combination of control prefectures, ensuring that the pre-treatment employment composition in the synthetic unit closely matches that of Miyagi. Figure 4 visualizes the employment compositions for Miyagi and control

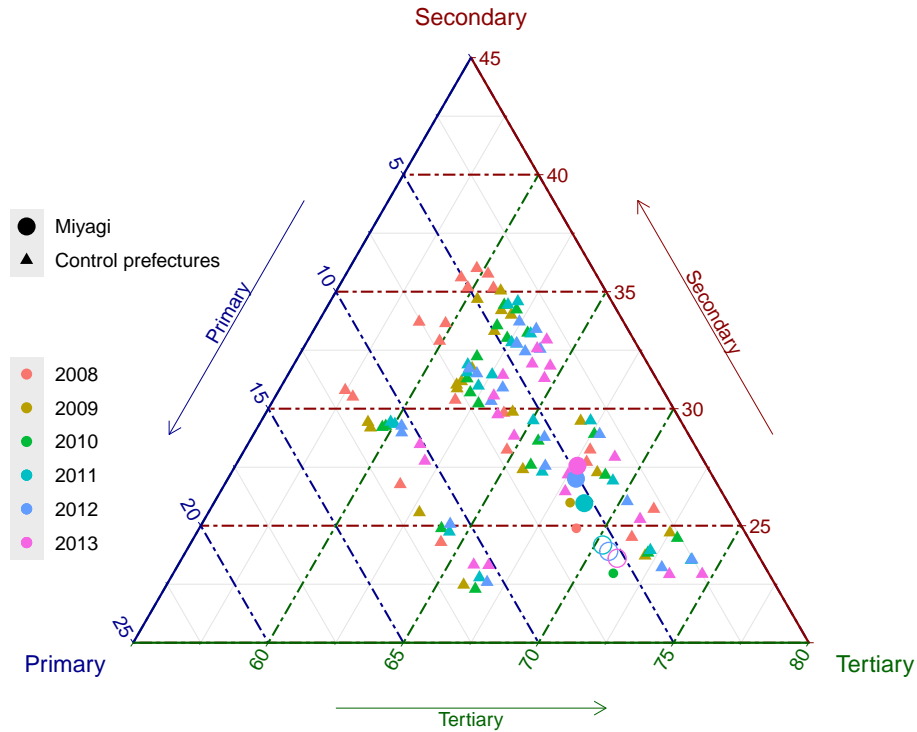


FIGURE 4. Ternary plot depicting employment compositions, where employment composition in the treated unit, Miyagi, is represented by circles, while employment compositions in the control prefectures are shown as triangles. Different years are distinguished by color. The synthetic controls for the post-treatment periods 2011, 2012 and 2013 are shown as hollow circles and are distinguished from the observed employment compositions for these years by a similar proportion of primary category employment, an increased proportion of secondary category employment and a reduced proportion of tertiary category employment.

prefectures using a ternary plot. The results indicate that the proportion of secondary category employment increased following the earthquake, while the proportion of tertiary category employment declined.

This shift is likely driven by large-scale reconstruction efforts. The destruction of infrastructure and housing spurred demand for construction-related jobs, leading to growth in secondary category employment. Meanwhile, many service-based businesses, particularly in retail and hospitality, faced prolonged disruptions due to physical damage, population displacement and reduced consumer demand. Additionally, some workers may have transitioned from the service sector to reconstruction-related employment, further contributing to the observed shift. These findings suggest that the earthquake temporarily reshaped the labor market, emphasizing reconstruction at the expense of service-oriented employment.

The observed employment compositions for Miyagi in the primary, secondary and tertiary category for 2011 are $(0.053, 0.260, 0.687)'$, for 2012 they are $(0.051, 0.270, 0.679)'$ and for 2013 they are $(0.048, 0.276, 0.676)'$, while the geodesic synthetic compositions obtained for the same years are $(0.055, 0.242, 0.703)'$, $(0.055, 0.239, 0.706)'$, and $(0.053, 0.236, 0.711)'$. The effect of the earthquake on employment composition appears to have been less pronounced in 2011, likely due to the timing of the disaster on March 11, 2011, with immediate disruptions offset by short-term stabilization efforts. The impact became more pronounced in 2012 and 2013, reflecting longer-term shifts in employment patterns. To assess the statistical significance of this effect, we applied the placebo permutation test described in Remark 3.3. The resulting p -values for the null hypothesis of no causal effect were 0.1 for 2011, 0.05 for 2012, and 0 for 2013. These results indicate that the immediate impact in 2011 was not strongly significant, but the earthquake’s effect on Miyagi’s employment composition became statistically significant starting from 2012.

5.2. Impact of the 1972 Abortion Legislation on Fertility Patterns in East Germany.

The study of fertility rates has attracted substantial attention, with an increasing emphasis on analyzing age-specific fertility rates (ASFR) rather than relying solely on summary measures such as total fertility rate (Chen et al., 2017). Represented as fertility curves across reproductive ages, ASFR provides richer insights into fertility behaviors, allowing researchers to detect age-specific causal effects that aggregate statistics alone cannot capture. For example, a policy intervention might disproportionately influence fertility behaviors among younger women, information that is lost when relying solely on aggregate metrics.

In March 1972, East Germany introduced legislation permitting women to terminate pregnancies within the first twelve weeks, significantly liberalizing abortion access. Although the primary intention was reproductive autonomy, an unintended consequence was a substantial drop in fertility, with the total fertility rate decreasing notably from 2.1 children per woman in 1971 to 1.5 by 1975 (Büttner and Lutz, 1990). To gain deeper insights into how this policy affected fertility behavior across different reproductive ages, we applied the proposed GSC to ASFR curves. When viewed as functions over reproductive ages, these are functional data in the space L^2 (see Example 2.5).

The data for this analysis were obtained from the Human Fertility Database, which provides ASFR annually for ages 12 to 55 for each calendar year across different countries. We select East Germany as the treated unit, given its distinct policy change, and utilize a control group composed of 26 countries that did not experience comparable abortion liberalization during this period (Austria, Belgium, Bulgaria, Belarus, Canada, Switzerland, Czechia, Denmark, Spain, Estonia, Finland, France, Hungary, Iceland, Ireland, Italy, Japan, Lithuania, Netherlands, Portugal, Russia, Slovakia, Sweden, Ukraine, United Kingdom (England and Wales), and United States). We define 1965–1971 as pre-treatment periods and 1972–1975 as post-treatment periods, so that it is possible to capture both immediate and medium-term policy impacts. Figure 5 visualizes the ASFR curves for East Germany and the control countries from 1966 to 1975 using heat maps. A clear reduction in fertility rates is evident for East Germany during the post-treatment period (1972–1975) but other countries also experience reductions in fertility between 1965 and 1975.

Figure 6 compares the observed ASFR of East Germany with the synthetic control unit constructed from the control countries. Visual inspection suggests that the synthetic control closely tracks East Germany’s pre-treatment fertility patterns. After the policy implementation in 1972, East Germany exhibits a notable downward shift in fertility rates across prime childbearing ages (approximately ages 20–30), as reflected in the divergence from the synthetic control unit.

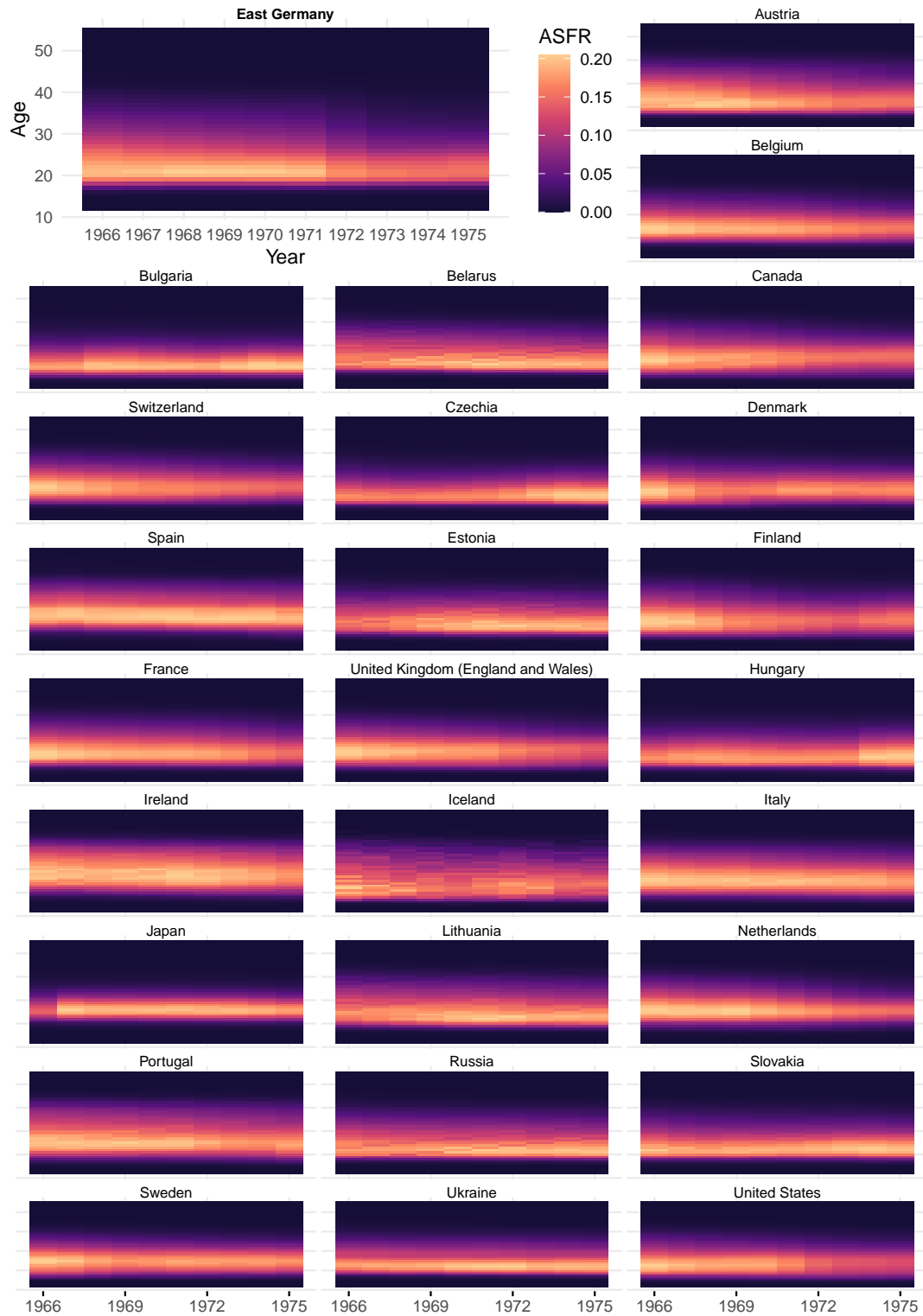


FIGURE 5. Age-specific fertility rates (ASFR) for East Germany and the control countries from 1966 to 1977 shown as heat maps. For each of the countries, each column represents the ASFR across ages 12 to 55 for a given calendar year that is indicated at the bottom of the figure.

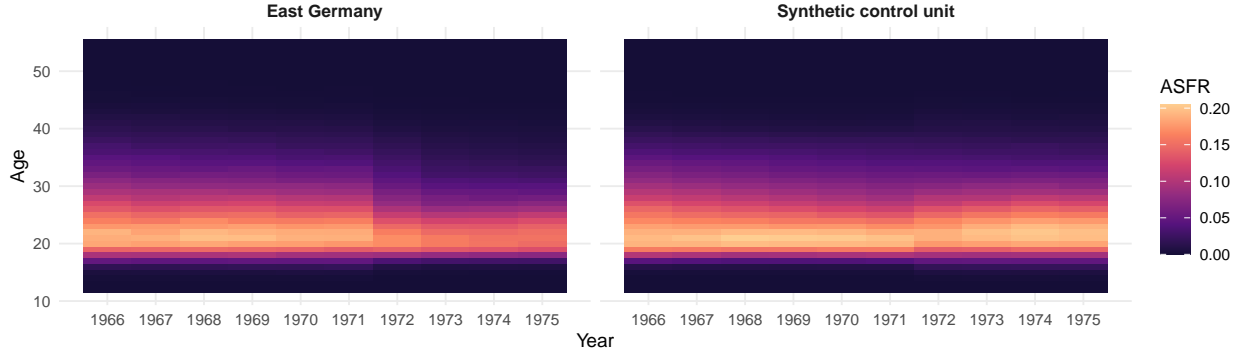


FIGURE 6. Heat maps of age-specific fertility rates (ASFR) for East Germany (left) and the synthetic control unit (right) from 1966 to 1975. Each column represents the ASFR across ages 12 to 55 (vertical axis) for each calendar year (horizontal axis).

To assess the statistical significance of these observed differences, we applied the placebo permutation test by repeatedly applying the synthetic control procedure to each control country as if it had been treated. The resulting p -values for the null hypothesis of no causal effect in each post-treatment year (1972–1975) are 0.15, 0.11, 0.00, and 0.04, respectively. These results indicate that the immediate impact in 1972 and 1973 is not strongly significant; however, the fertility reduction becomes statistically significant in 1974. This confirms that the 1972 abortion policy had a substantial causal effect on fertility behavior in East Germany.

6. EXTENSION TO GEODESIC SYNTHETIC DIFFERENCE-IN-DIFFERENCES

6.1. Construction of the estimator. We discuss an extension of synthetic difference-in-differences developed in [Arkhangelsky et al. \(2021\)](#) for the Euclidean case to outcomes located in geodesic metric spaces. Define

$$Y_{j,T_0+1:T}^{(\oplus)} = \arg \min_{\nu \in \mathcal{M}} \frac{1}{T - T_0} \sum_{t=T_0+1}^T d^2(\nu, Y_{j,t}), \quad j = 1, \dots, J + 1,$$

$$Y_{1,T_0+1:T}(D) = \arg \min_{\nu \in \mathcal{M}} \frac{1}{T - T_0} \sum_{t=T_0+1}^T d^2(\nu, Y_{1,t}(D)), \quad D \in \{N, I\}.$$

In what follows, the causal effect of interest is the geodesic τ from $Y_{1,T_0+1:T}^{(\oplus)}(N)$ to $Y_{1,T_0+1:T}^{(\oplus)}(I)$,

$$\tau = \gamma_{Y_{1,T_0+1:T}^{(\oplus)}(N), Y_{1,T_0+1:T}^{(\oplus)}(I)}.$$

Aiming at a geodesic synthetic difference-in-differences (GSDID) estimator, we introduce a vector of weights λ indexed by time in addition to the previously introduced vector of weights w indexed by units. For non-negative weight vectors in the simplex $w \in \Delta^{J-1}$, $\lambda \in \Delta^{T_0-1}$, $t = 1, \dots, T_0$, and $j = 1, \dots, J + 1$, define

$$Y_{2:J+1,t}^{(w)} = \arg \min_{\nu \in \mathcal{M}} \sum_{j=2}^{J+1} w_j d^2(\nu, Y_{j,t}), \quad Y_{j,1:T_0}^{(\lambda)} = \arg \min_{\nu \in \mathcal{M}} \sum_{t=1}^{T_0} \lambda_t d^2(\nu, Y_{j,t}),$$

$$Y_{2:J+1,1:T_0}^{(\mathbf{w},\boldsymbol{\lambda})} = \arg \min_{\nu \in \mathcal{M}} \sum_{j=2}^{J+1} w_j d^2(\nu, Y_{j,1:T_0}^{(\boldsymbol{\lambda})}), \quad Y_{2:J+1,T_0+1:T}^{(\mathbf{w},\oplus)} = \arg \min_{\nu \in \mathcal{M}} \sum_{j=2}^{J+1} w_j d^2(\nu, Y_{j,T_0+1:T}^{(\oplus)}).$$

With $\Gamma_{\alpha,\beta} : \mathcal{M} \rightarrow \mathcal{M}$ denoting a geodesic transport map for $\alpha, \beta \in \mathcal{M}$ as introduced in Assumption 3.2, we define the GSDID estimator for τ as

$$\tau^{(\text{GSDID})} = \gamma_{Y_{1,T_0+1:T}^{(\text{GSDID})}, Y_{1,T_0+1:T}^{(\oplus)}},$$

where

$$Y_{1,T_0+1:T}^{(\text{GSDID})} = \Gamma_{Y_{2:J+1,1:T_0}^{(\bar{\mathbf{w}},\bar{\boldsymbol{\lambda}})}, Y_{2:J+1,T_0+1:T}^{(\bar{\mathbf{w}},\oplus)}} \left(Y_{1,1:T_0}^{(\bar{\boldsymbol{\lambda}})} \right),$$

$$\bar{\mathbf{w}} \in \arg \min_{\mathbf{w} \in \Delta^{J-1}} \frac{1}{T_0} \sum_{t=1}^{T_0} d^2(Y_{1,t}, Y_{2:J+1,t}^{(\mathbf{w})}), \quad \bar{\boldsymbol{\lambda}} \in \arg \min_{\boldsymbol{\lambda} \in \Delta^{T_0-1}} \frac{1}{J} \sum_{j=2}^{J+1} d^2(Y_{j,T_0+1:T}^{(\oplus)}, Y_{j,1:T_0}^{(\boldsymbol{\lambda})}).$$

Note that for the special case of Euclidean outcomes, the proposed GSDID estimator becomes

$$Y_{1,T_0+1:T}^{(\text{GSDID})} = Y_{1,1:T_0}^{(\bar{\boldsymbol{\lambda}})} + \left(Y_{2:J+1,T_0+1:T}^{(\bar{\mathbf{w}},\oplus)} - Y_{2:J+1,1:T_0}^{(\bar{\mathbf{w}},\bar{\boldsymbol{\lambda}})} \right)$$

$$= \sum_{t=1}^{T_0} \bar{\lambda}_t Y_{1,t} + \left(\frac{1}{T - T_0} \sum_{t=T_0+1}^T \sum_{j=2}^{J+1} \bar{w}_j Y_{j,t} - \sum_{t=1}^{T_0} \sum_{j=2}^{J+1} \bar{w}_j \bar{\lambda}_t Y_{j,t} \right),$$

which is the SDID estimator of [Arkhangelsky et al. \(2021\)](#). Thus, the proposed estimator is a natural extension of the established case with Euclidean outcomes. We discuss extensions to cases with multiple treated units or where the interest lies in the causal effects at multiple post-treatment time points in Remark 6.3 below.

Remark 6.1 (*Connection with geodesic synthetic control method and geodesic difference-in-differences*). To discuss the relation of the proposed GSDID estimator with the GSC estimator introduced above and the geodesic DID (GDID) estimator introduced in [Zhou et al. \(2025\)](#), we note that GSC, GDID, and GSDID estimators can be represented as geodesic transports based on weighted averages of outcomes $\delta_{j,k}^{(M)}$, $k = 1, 2, 3$, using appropriate weights $w_j^{(M)}$, $M \in \{\text{GSC}, \text{GDID}, \text{GSDID}\}$, i.e.,

$$\tau^{(M)} := \gamma_{Y_{1,T_0+1:T}^{(M)}, Y_{1,T_0+1:T}^{(\oplus)}}$$

where

$$Y_{1,T_0+1:T}^{(M)} = \Gamma_{\delta_{2:J+1,1:T_0}^{(M)}, \delta_{2:J+1,T_0+1:T}^{(M)}} \left(\delta_{1,1:T_0}^{(M)} \right), \quad \delta_{2:J+1,1:T_0}^{(M)} = \arg \min_{\nu \in \mathcal{M}} \sum_{j=2}^{J+1} w_j^{(M)} d^2(\nu, \delta_{j,1:T_0}^{(M)}),$$

$$\delta_{2:J+1,T_0+1:T}^{(M)} = \arg \min_{\nu \in \mathcal{M}} \sum_{j=2}^{J+1} w_j^{(M)} d^2(\nu, \delta_{j,T_0+1:T}^{(M)}), \quad \delta_{1,1:T_0}^{(M)} = \arg \min_{\nu \in \mathcal{M}} \sum_{j=2}^{J+1} w_j^{(M)} d^2(\nu, \bar{\delta}_{j,1:T_0}^{(M)}),$$

and

$$\{w_j^{(\text{GSC})}, \delta_{j,1:T_0}^{(\text{GSC})}, \delta_{j,T_0+1:T}^{(\text{GSC})}, \bar{\delta}_{j,1:T_0}^{(\text{GSC})}\} = \{\bar{w}_j, Y_{j,1:T_0}^{(\oplus)}, Y_{j,T_0+1:T}^{(\oplus)}, Y_{j,1:T_0}^{(\oplus)}\},$$

$$\{w_j^{(\text{GDID})}, \delta_{j,1:T_0}^{(\text{GDID})}, \delta_{j,T_0+1:T}^{(\text{GDID})}, \bar{\delta}_{j,1:T_0}^{(\text{GDID})}\} = \left\{ \frac{1}{J}, Y_{j,1:T_0}^{(\oplus)}, Y_{j,T_0+1:T}^{(\oplus)}, Y_{1,1:T_0}^{(\oplus)} \right\},$$

$$\{w_j^{(\text{GSDID})}, \delta_{j,1:T_0}^{(\text{GSDID})}, \delta_{j,T_0+1:T}^{(\text{GSDID})}, \bar{\delta}_{j,1:T_0}^{(\text{GSDID})}\} = \{\bar{w}_j, Y_{j,1:T_0}^{(\bar{\boldsymbol{\lambda}})}, Y_{j,T_0+1:T}^{(\oplus)}, Y_{1,1:T_0}^{(\bar{\boldsymbol{\lambda}})}\}.$$

Specifically, setting $T = T_0 + 1$ for the GSC and setting $T_0 = 1$, $T = 2$ for the GDID, we have

$$Y_{1,T_0+1:T}^{(\text{GSC})} = \Gamma_{Y_{2:J+1,1:T_0}, Y_{2:J+1,T_0+1}}^{(\bar{w}, \oplus)} \left(Y_{2:J+1,1:T_0}^{(\bar{w}, \oplus)} \right) = Y_{2:J+1,T_0+1}^{(\bar{w})}, \quad (6.1)$$

$$Y_{1,T_0+1:T}^{(\text{GDID})} = \Gamma_{Y_{2:J+1,1}, Y_{2:J+1,2}}^{(\oplus)} (Y_{1,1}), \quad (6.2)$$

where

$$Y_{2:J+1,t}^{(\oplus)} = \arg \min_{\nu \in \mathcal{M}} \frac{1}{J} \sum_{j=2}^{J+1} d^2(\nu, Y_{j,t}), \quad t = 1, 2.$$

The resulting estimators (6.1) and (6.2) coincide with the GSC and GDID estimators, respectively. Under Assumption 6.2 below, we have $Y_{1,T_0+1}^{(\text{GSC})} = Y_{1,T_0+1}(N)$. Comparing $\{\delta_{j,1:T_0}^{(\text{GSC})}, \bar{\delta}_{j,1:T_0}^{(\text{GSC})}\}$ and $\{\delta_{j,1:T_0}^{(\text{GSDID})}, \bar{\delta}_{j,1:T_0}^{(\text{GSDID})}\}$, the GSDID can be interpreted as attenuating the bias of the GSC estimator by introducing additional flexibility through the weights $\bar{\lambda}$ that are not present in the GSC. Under Assumption 6.3 below, we have $Y_{1,2}^{(\text{GDID})} = Y_{1,2}(N)$. Comparing the weights $w_j^{(\text{GDID})}$ and $w_j^{(\text{GSDID})}$, GSDID can be seen as introducing additional flexibility to estimate the target $Y_{1,T_0+1:T}^{(\oplus)}(N)$ through the weights \bar{w} , which may attenuate bias when the parallelity assumption does not hold. The proposed GSDID thus emerges as a method that combines favorable properties of both GSC and GDID.

6.2. Causal model for geodesic synthetic difference-in-differences. Consider the following model for potential outcomes without intervention:

$$Y_{j,t}(N) = g(U_j, V_t), \quad t = 1, \dots, T, \quad j = 1, \dots, J+1, \quad (6.3)$$

where $(U_j, V_t) \in \mathcal{M} \times \mathcal{M}$ is a pair of unobservable characteristics of unit j at time t and $g(\cdot, \cdot) : \mathcal{M} \times \mathcal{M} \rightarrow \mathcal{M}$ is a measurable function, where \mathcal{M} is the geodesic metric space where the outcomes are located. Define

$$g^{(\oplus)}(U_j, V_{T_0+1:T}) = \arg \min_{\nu \in \mathcal{M}} \frac{1}{T - T_0} \sum_{t=T_0+1}^T d^2(\nu, g(U_j, V_t)).$$

For non-negative weight vectors in the simplex $\mathbf{w} \in \Delta^{J-1}$ and $\boldsymbol{\lambda} \in \Delta^{T_0-1}$, we additionally define

$$g^{(\boldsymbol{\lambda})}(U_j, V_{1:T_0}) = \arg \min_{\nu \in \mathcal{M}} \sum_{t=1}^{T_0} \lambda_t d^2(\nu, g(U_j, V_t)),$$

$$g^{(\mathbf{w})}(U_{2:J+1}, V_t) = \arg \min_{\nu \in \mathcal{M}} \sum_{j=2}^{J+1} w_j d^2(\nu, g(U_j, V_t)),$$

$$g^{(\mathbf{w}, \oplus)}(U_{2:J+1}, V_{T_0+1:T}) = \arg \min_{\nu \in \mathcal{M}} \sum_{j=2}^{J+1} w_j d^2(\nu, g^{(\oplus)}(U_j, V_{T_0+1:T})),$$

$$g^{(\mathbf{w}, \boldsymbol{\lambda})}(U_{2:J+1}, V_{1:T_0}) = \arg \min_{\nu \in \mathcal{M}} \sum_{j=2}^{J+1} w_j d^2(\nu, g^{(\boldsymbol{\lambda})}(U_j, V_{1:T_0})).$$

We impose the following assumptions.

Assumption 6.1. *For any $\mathbf{w} \in \Delta^{J-1}$ and $\boldsymbol{\lambda} \in \Delta^{T_0-1}$, the objects $g^{(\boldsymbol{\lambda})}(U_j, V_{1:T_0})$, $g^{(\oplus)}(U_j, V_{T_0+1:T})$, $g^{(\mathbf{w})}(U_{2:J+1}, V_j)$, $g^{(\mathbf{w}, \oplus)}(U_{2:J+1}, V_{T_0+1:T})$, and $g^{(\mathbf{w}, \boldsymbol{\lambda})}(U_{2:J+1}, V_{1:T_0})$ exist and are unique.*

For $t = 1, \dots, T_0$ and $j = 1, \dots, J + 1$, define

$$\mathbb{W}_t^* = \{\mathbf{w}^* \in \Delta^{J-1} : d(g(U_1, V_t), g^{(\mathbf{w}^*)}(U_{2:J+1}, V_t)) = \inf_{\mathbf{w} \in \Delta^{J-1}} d(g(U_1, V_t), g^{(\mathbf{w})}(U_{2:J+1}, V_t))\},$$

$$\Lambda_j^* = \left\{ \boldsymbol{\lambda}^* \in \Delta^{T_0-1} : d(g^{(\oplus)}(U_j, V_{T_0+1:T}), g^{(\boldsymbol{\lambda}^*)}(U_j, V_{1:T_0})) = \inf_{\boldsymbol{\lambda} \in \Delta^{T_0-1}} d(g^{(\oplus)}(U_j, V_{T_0+1:T}), g^{(\boldsymbol{\lambda})}(U_j, V_{1:T_0})) \right\}.$$

Assumption 6.2 (Synthetic control).

- (i) For $t = 1, \dots, T_0$, $\mathbb{W}_t^* = \{\mathbf{w} \in \Delta^{J-1} : d(g(U_1, V_t), g^{(\mathbf{w})}(U_{2:J+1}, V_t)) = 0\}$ and $\bigcap_{t=1}^{T_0} \mathbb{W}_t^*$ is not empty.
- (ii) The set $\bigcap_{j=2}^{J+1} \Lambda_j^*$ is not empty. For any $\boldsymbol{\lambda} \in \bigcap_{j=2}^{J+1} \Lambda_j^*$, $\bigcap_{t=1}^{T_0} \mathbb{W}_t^* \subset \mathbb{W}_{\boldsymbol{\lambda}}^* \cap \mathbb{W}_{\oplus}^*$ where

$$\mathbb{W}_{\boldsymbol{\lambda}}^* = \left\{ \mathbf{w} \in \Delta^{J-1} : d(g^{(\boldsymbol{\lambda})}(U_1, V_{1:T_0}), g^{(\mathbf{w}, \boldsymbol{\lambda})}(U_{2:J+1}, V_{1:T_0})) = 0 \right\},$$

$$\mathbb{W}_{\oplus}^* = \left\{ \mathbf{w} \in \Delta^{J-1} : d(g^{(\oplus)}(U_1, V_{T_0+1:T}), g^{(\mathbf{w}, \oplus)}(U_{2:J+1}, V_{T_0+1:T})) = 0 \right\}.$$

Assumption 6.3 (Parallel trend).

- (i) The set $\bigcap_{j=2}^{J+1} \Lambda_j^*$ is not empty and $\bigcap_{j=2}^{J+1} \Lambda_j^* \subset \Lambda_1^*$.
- (ii) The set $\bigcap_{t=1}^{T_0} \mathbb{W}_t^*$ is not empty. For any $\mathbf{w} \in \bigcap_{t=1}^{T_0} \mathbb{W}_t^*$, $\boldsymbol{\lambda}_2 \in \bigcap_{j=2}^{J+1} \Lambda_j^*$ and $\boldsymbol{\lambda}_1 \in \Lambda_1^*$,

$$\Gamma_{\alpha, \beta} \left(g^{(\boldsymbol{\lambda}_1)}(U_1, V_{1:T_0}) \right) = g^{(\oplus)}(U_1, V_{T_0+1:T}),$$

where $\alpha = g^{(\mathbf{w}, \boldsymbol{\lambda}_2)}(U_{2:J+1}, V_{1:T_0})$ and $\beta = g^{(\mathbf{w}, \oplus)}(U_{2:J+1}, V_{T_0+1:T})$.

Assumption 6.2 is for the GSC. Assumption 6.2 (ii) implies that the optimal weights \mathbf{w} such that $Y_{2:J+1,t}^{(\mathbf{w})} = Y_{1,t}(N)$ at each time point $t = 1, \dots, T_0$ are still optimal in the sense that $Y_{1,1:T_0}^{(\boldsymbol{\lambda})}(N)$ and $Y_{1,T_0+1:T}^{(\oplus)}(N)$ respectively coincide with $Y_{2:J+1,1:T_0}^{(\mathbf{w}, \boldsymbol{\lambda})}(N)$ and $Y_{2:J+1,T_0+1:T}^{(\mathbf{w}, \oplus)}(N)$ as long as $\boldsymbol{\lambda}$ belongs to the set of optimal weights $\bigcap_{j=2}^{J+1} \Lambda_j^*$ such that for $j = 2, \dots, J+1$, $Y_{j,1:T_0}^{(\boldsymbol{\lambda})}$ is the closest to $Y_{j,T_0+1:T}^{(\oplus)}(N)$ with respect to the metric d among the Fréchet means $Y_{j,1:T_0}^{(\boldsymbol{\lambda}_0)}$ with $\boldsymbol{\lambda}_0 \in \Delta^{T_0-1}$. Figure 7 illustrates the GSDID under Assumption 6.2.

Assumption 6.3 (ii) corresponds to the parallel trend assumption for the GDID. We refer to Zhou et al. (2025) for more details about its construction and theoretical properties. For Euclidean outcomes, Assumption 6.3 (ii) reduces to

$$g^{(\boldsymbol{\lambda}_1)}(U_1, V_{1:T_0}) + \{g^{(\mathbf{w}, \oplus)}(U_{2:J+1}, V_{T_0+1:T}) - g^{(\mathbf{w}, \boldsymbol{\lambda}_2)}(U_{2:J+1}, V_{1:T_0})\} = g^{(\oplus)}(U_1, V_{T_0+1:T}),$$

which corresponds to the standard assumption of parallel trends in the canonical DID framework (Zhou et al., 2025). Figure 8 illustrates the GSDID under Assumption 6.3.

For the space of networks (Example 2.1), Wasserstein space (Example 2.4), the space of functional data (Example 2.5), and the space of SPD matrices (Example 2.3) with either the Frobenius metric, the power metric family, the Log-Euclidean metric or the Log-Cholesky metric, one can verify Assumptions 6.1, 6.2, and 6.3 (i). Indeed, letting $g(U_j, V_t) = \gamma_{U_j, V_t}(\alpha)$, $\alpha \in (0, 1)$,

$$g^{(\mathbf{w}, \boldsymbol{\lambda})}(U_{2:J+1}, V_{1:T_0}) = \gamma_{U_{2:J+1}, V_{1:T_0}}^{(\boldsymbol{\lambda})}(\alpha), \quad g^{(\mathbf{w}, \oplus)}(U_{2:J+1}, V_{T_0+1:T}) = \gamma_{U_{2:J+1}, V_{T_0+1:T}}^{(\oplus)}(\alpha)$$

for any $\mathbf{w} \in \Delta^{J-1}$ and any $\boldsymbol{\lambda} \in \Delta^{T_0-1}$, where

$$U_{2:J+1}^{(\mathbf{w})} = \arg \min_{\nu \in \mathcal{M}} \sum_{j=2}^{J+1} w_j d^2(\nu, U_j),$$

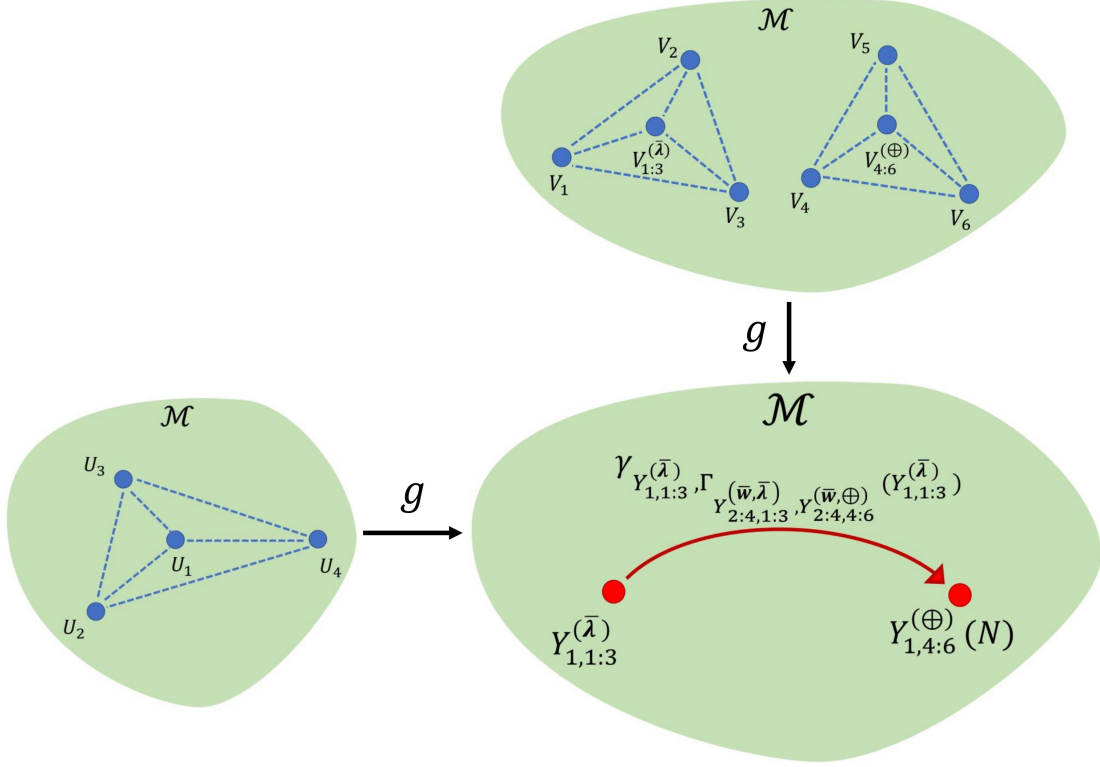


FIGURE 7. Illustration of geodesic synthetic difference-in-differences under Assumption 6.2. The circles symbolize objects in the geodesic metric space \mathcal{M} . Under Assumption 6.2, $Y_{2:4,1:3}^{(\bar{w}, \bar{\lambda})} = Y_{1,1:3}^{(\bar{\lambda})}$ and $Y_{2:4,4:6}^{(\bar{w}, \oplus)} = Y_{1,4:6}^{(\oplus)}$. The solid red arrow is the geodesic from $Y_{1,1:3}^{(\bar{\lambda})}$ to $Y_{1,4:6}^{(\oplus)}(N)$, representing the bias correction for geodesic synthetic controls as effected by geodesic synthetic difference-in-differences.

$$V_{T_0+1:T}^{(\oplus)} = \arg \min_{\nu \in \mathcal{M}} \frac{1}{T - T_0} \sum_{t=T_0+1}^T d^2(\nu, V_t), \quad V_{1:T_0}^{(\lambda)} \in \arg \min_{\nu \in \mathcal{M}} \sum_{t=1}^{T_0} \lambda_t d^2(\nu, V_t).$$

For the space of compositional data (Example 2.2), consider the causal model $g(U_j, V_t) = \text{Exp}_{V_t}(\text{Log}_{U_1}(U_j))$. If we additionally assume that

$$g^{(\lambda)}(U_j, V_{1:T_0}) = \text{Exp}_{V_{1:T_0}^{(\lambda)}}(\text{Log}_{U_1}(U_j)), \quad g^{(\oplus)}(U_j, V_{T_0+1:T}) = \text{Exp}_{V_{T_0+1:T}^{(\oplus)}}(\text{Log}_{U_1}(U_j))$$

for any $j = 1, \dots, J + 1$ and any $\lambda \in \Delta^{T_0-1}$, Assumptions 6.1, 6.2, and 6.3 (i) can be verified.

The following result establishes the identification of the GSDID estimator.

Theorem 6.1. *Suppose that Assumptions 3.2 and 6.1 hold for the model (6.3). Then under Assumption 6.2 or 6.3, we have*

$$Y_{1, T_0+1:T}^{(\text{GSDID})} = Y_{1, T_0+1:T}^{(\oplus)}(N). \quad (6.4)$$

Theorem 6.1 provides a type of double robustness property of the GSDID estimator. Specifically, even if the weights \bar{w} for GSC or $\bar{\lambda}$ for GDID fail to remove the bias of the method, the combination of weights can compensate for this. This double robustness property corresponds to the double

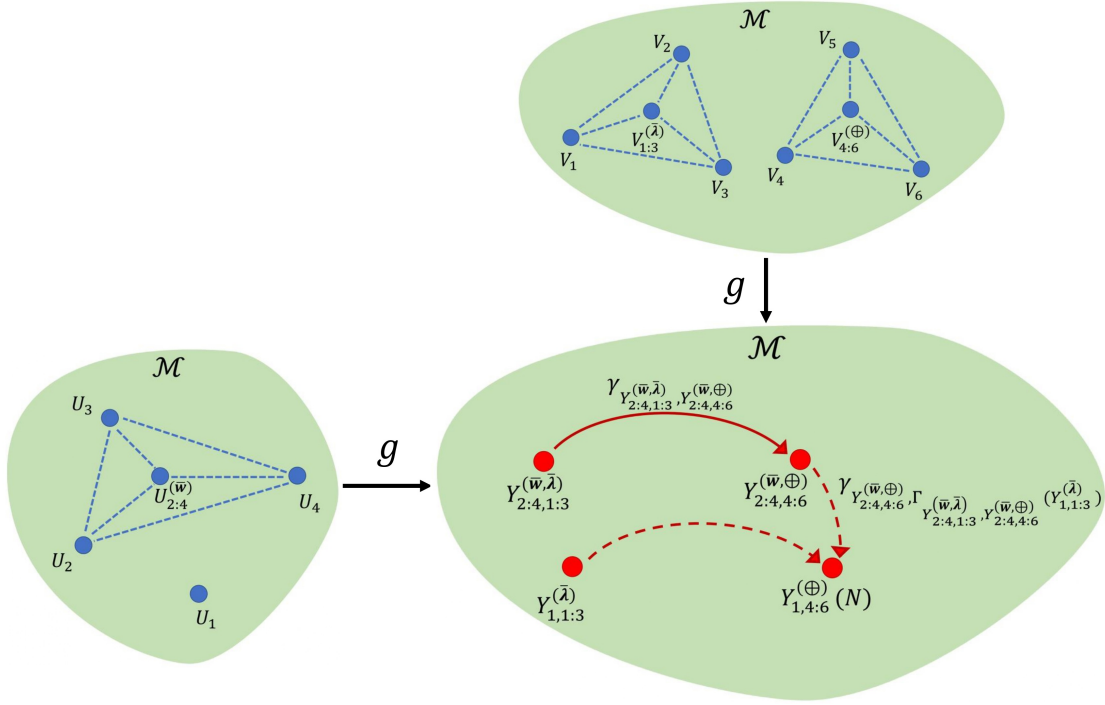


FIGURE 8. Illustration of GSDID under Assumption 6.3. The circles symbolize objects in the geodesic metric space \mathcal{M} . Arrows depict geodesics connecting them. The dashed red arrow from $Y_{1,1:3}^{(\bar{\lambda})}$ to $Y_{1,4:6}^{(\oplus)}(N)$ represents the trend between pre-treatment and post-treatment for unit 1. The solid red arrow represents the parallel trend. The dashed red arrow from $Y_{2:4,4:6}^{(\bar{w}, \oplus)}$ to $Y_{1,4:6}^{(\oplus)}(N)$ represents the bias correction of the GSC affected by the GSDID.

robustness property of synthetic DID for Euclidean outcomes and is similar to the property of the augmented inverse probability weighting estimator for Euclidean outcomes, demonstrating the possibility of trading off the accuracy of the outcome model and the treatment assignment model. We refer to Kurisu et al. (2024) for further discussion of the augmented inverse probability weighting estimator and its double robustness for outcomes taking values in geodesic metric spaces.

Remark 6.2 (*Placebo permutation test*). We can also employ a placebo permutation test for GSDID. We first compute $Y_{j, T_0+1:T}^{(\text{GSDID})}$ for $j = 2, \dots, J + 1$ by applying the same algorithm to obtain $Y_{1, T_0+1:T}^{(\text{GSDID})}$ by pretending the treated unit is j . The p -value for the null hypothesis of no causal effect by the intervention to unit $j = 1$ is given by

$$\frac{\text{rank of } d(Y_{1, T_0+1:T}^{(\oplus)}, Y_{1, T_0+1:T}^{(\text{GSDID})}) \text{ in } \{d(Y_{j, T_0+1:T}^{(\oplus)}, Y_{j, T_0+1:T}^{(\text{GSDID})}) : j = 1, \dots, J + 1\}}{J + 1}.$$

Remark 6.3 (*Extensions*). The GSDID estimator can be extended in several directions. First, if one is interested in causal effects at different time points, one can replace $Y_{2:J+1, 1:T_0}^{(\bar{w}, \bar{\lambda})}$ and $Y_{1, 1:T_0}^{(\bar{\lambda})}$ in

the definition of $Y_{1,T_0+1:T}^{(\text{GSDID})}$ with $Y_{2:J+1,1:T_0}^{(\bar{w},\bar{\lambda}_t)}$ and $Y_{1,1:T_0}^{(\bar{\lambda}_t)}$, respectively, where

$$\bar{\lambda}_t \in \arg \min_{\lambda \in \Delta^{T_0-1}} \frac{1}{J} \sum_{j=2}^{J+1} d^2(Y_{j,t}, Y_{j,1:T_0}^{(\lambda)}), \quad t = T_0 + 1, \dots, T.$$

In this case, the causal effects of interest are given by $\gamma_{Y_{1,t}(N), Y_{1,t}(I)}$ for $t = T_0 + 1, \dots, T$.

Second, if there are multiple treated units, say $\{(Y_{11,t}, \dots, Y_{1K,t})\}_{t=1}^T$ instead of $\{Y_{1,t}\}_{t=1}^T$, one can replace $Y_{1,1:T_0}^{(\bar{\lambda})}$ in the definition of $Y_{1,T_0+1:T}^{(\text{GSDID})}$ with $Y_{1,1:K,1:T_0}^{(\bar{\lambda}, \oplus)}$ for the implementation of the GSDID, where

$$Y_{1,1:K,1:T_0}^{(\lambda, \oplus)} = \arg \min_{\nu \in \mathcal{M}} \sum_{t=1}^{T_0} \lambda_t d^2(\nu, Y_{1,1:K,t}^{(\oplus)}), \quad Y_{1,1:K,t}^{(\oplus)} = \arg \min_{\nu \in \mathcal{M}} \frac{1}{K} \sum_{j=1}^K d^2(\nu, Y_{1j,t}).$$

If $Y_{1j,t}(I)$ and $Y_{1j,t}(N)$ denote potential outcomes of the j -th treated unit at time t with and without intervention, respectively, the causal effect of interest is given by

$$\gamma_{Y_{1,1:K,T_0+1:T}^{(\oplus, \oplus)}(N), Y_{1,1:K,T_0+1:T}^{(\oplus, \oplus)}(I)},$$

where

$$Y_{1,1:K,T_0+1:T}^{(\oplus, \oplus)}(D) = \arg \min_{\nu \in \mathcal{M}} \frac{1}{T - T_0} \sum_{t=T_0+1}^T d^2(\nu, Y_{1,1:K,t}^{(\oplus)}(D)), \quad D \in \{N, I\},$$

$$Y_{1,1:K,t}^{(\oplus)}(D) = \arg \min_{\nu \in \mathcal{M}} \frac{1}{K} \sum_{j=1}^K d^2(\nu, Y_{1j,t}(D)).$$

Third, if one is interested in causal effects at different time points with multiple treated units, one can replace $Y_{1,1:T_0}^{(\bar{\lambda})}$ in the definition of $Y_{1,T_0+1:T}^{(\text{GSDID})}$ with $Y_{1,1:K,1:T_0}^{(\bar{\lambda}_t, \oplus)}$. In this case, the causal effects of interest are given by

$$\gamma_{Y_{1,1:K,t}^{(\oplus)}(N), Y_{1,1:K,t}^{(\oplus)}(I)}, \quad t = T_0 + 1, \dots, T.$$

By appropriately modifying Assumptions 6.1–6.3, it is also possible to extend Theorem 6.1 to the case with multiple treated units. Further combinations of times and treated units are possible and can be handled analogously.

6.3. Analysis of the effect of the collapse of the Soviet Union on mortality with geodesic synthetic difference-in-differences. The collapse of the Soviet Union in 1991 led to severe economic and social disruptions, profoundly affecting mortality patterns in Russia. The transition from a centrally planned economy to a market-based system was marked by economic instability, rising unemployment, healthcare system deterioration, and increased alcohol consumption, all of which contributed to a dramatic decline in life expectancy. Between 1990 and 1994, life expectancy for Russian men fell from 63.8 to 57.6 years, while for women, it declined from 74.4 to 71.0 years (Notzon et al., 1998). Rather than relying solely on summary measures such as life expectancy, a more comprehensive understanding of this demographic shock requires a more detailed analysis, which motivates the analysis of entire age-at-death distributions.

The data supporting such an analysis is available from the [Human Mortality Database](#), which provides life tables with 5-year time intervals for multiple countries, including Russia and various Western European countries. These life tables are sorted by age and calendar year and can easily be converted into age-at-death distributions. Specifically, for each country, we obtain age-at-death

distributions by constructing their probability densities through slightly smoothing the histograms of the age-at-death distribution obtained from the available life table data. For this preprocessing step we use the `CreateDensity` function from the `frechet` package (Chen et al., 2023b).

We treat Russia as the intervention unit, while the control group consists of 19 Western European countries: Austria, Belgium, Denmark, Finland, France, Germany, Greece, Iceland, Ireland, Italy, Luxembourg, Netherlands, Norway, Portugal, Slovenia, Spain, Sweden, Switzerland, and the United Kingdom. For this analysis, we apply the geodesic synthetic difference-in-differences model (GSDID) as delineated in Sections 6.1 and 6.2. to estimate the causal effect of the Soviet Union’s collapse on Russia’s age-at-death distribution using the Wasserstein metric (see Example 2.4).

Details on the implementation of GSDID are in Algorithm 2. The optimization problems in Steps 1 and 2 of Algorithm 2 are addressed in a similar way to those in Step 1 of Algorithm 1. The third step of Algorithm 2 involves constructing the geodesic transport map, with details provided in Remark 3.5.

We consider four time periods: 1980–1984 and 1985–1989 as pre-treatment periods, and 1990–1994 and 1995–1999 as post-treatment periods, with the Soviet collapse occurring in 1991. The effects of the collapse are expected to be extended over time. Figure 9 illustrates the available data through the estimated probability densities of the age-at-death distributions for males and females in Russia and the control countries. In Russia, a clear leftward shift is observed in the post-treatment periods (1990–1994 and 1995–1999), indicating increased mortality and a decline in longevity. This shift is especially pronounced for males, reflecting a substantial reduction in survival probabilities at younger and middle ages.

When applying GSDID, we reweigh the control countries to ensure that their pre-treatment time trends align with those of Russia, allowing for a difference-in-differences analysis within the geodesic framework. Figure 10 presents the observed and synthetic post-treatment age-at-death densities for both males and females. The GSDID framework captures not only the overall reduction in life expectancy but also the complex age- and gender-specific effects of the economic and societal shocks that resulted from the collapse of the Soviet Union. The results confirm that the collapse caused a significant leftward shift in Russia’s age-at-death distribution, with sharply increased mortality risk across multiple age groups. The effect was particularly severe for males, reflected in a more pronounced leftward shift. A plausible explanation for this gender disparity is the heightened vulnerability of working-age men to economic collapse, labor market instability and increased alcohol-related mortality.

To assess the statistical significance of this effect, we apply the placebo permutation test described in Remark 6.2. This procedure constructs synthetic age-at-death distributions for each control country by pretending it was treated, allowing us to evaluate whether the observed shift in Russia’s mortality patterns is extreme compared to placebo assignments. The resulting p -values for the null hypothesis of no causal effect are 0 for both females and males. These findings provide strong evidence that the collapse of the Soviet Union indeed caused a substantial and statistically significant impact on mortality for nearly all age groups in Russia.

7. CONCLUDING REMARKS

A general causal model for outcomes that can be viewed as random objects, i.e., elements located in a suitable geodesic metric space, is the proposed geodesic synthetic difference-in-differences model

Algorithm 2: Geodesic Synthetic Difference-in-Differences

Input: data $\{Y_{j,t} : j = 1, \dots, J+1, t = 1, \dots, T\}$.

Output: geodesic synthetic difference-in-differences estimator $\tau^{(\text{GSDID})}$.

- 1 $\bar{\mathbf{w}} = (\bar{w}_2, \dots, \bar{w}_{J+1}) \leftarrow$ the estimated unit weights:

$$\bar{\mathbf{w}} \in \arg \min_{\mathbf{w} \in \Delta^{J-1}} \frac{1}{T_0} \sum_{t=1}^{T_0} d^2(Y_{1,t}, Y_{2:J+1,t}^{(\mathbf{w})}),$$

where $Y_{2:J+1,t}^{(\mathbf{w})} = \arg \min_{\nu \in \mathcal{M}} \sum_{j=2}^{J+1} w_j d^2(\nu, Y_{j,t})$ for $t = 1, \dots, T_0$;

- 2 $\bar{\boldsymbol{\lambda}} = (\bar{\lambda}_1, \dots, \bar{\lambda}_{T_0}) \leftarrow$ the estimated time weights:

$$\bar{\boldsymbol{\lambda}} = \arg \min_{\boldsymbol{\lambda} \in \Delta^{T_0-1}} \frac{1}{J} \sum_{j=2}^{J+1} d^2(Y_{j,T_0+1:T}^{(\oplus)}, Y_{j,1:T_0}^{(\boldsymbol{\lambda})}),$$

where

$$Y_{j,T_0+1:T}^{(\oplus)} = \arg \min_{\nu \in \mathcal{M}} \frac{1}{T - T_0} \sum_{t=T_0+1}^T d^2(\nu, Y_{j,t}),$$

$$Y_{j,1:T_0}^{(\boldsymbol{\lambda})} = \arg \min_{\nu \in \mathcal{M}} \sum_{t=1}^{T_0} \lambda_t d^2(\nu, Y_{j,t})$$

for $j = 1, \dots, J+1$;

- 3 $Y_{1,T_0+1:T}^{(\text{GSDID})} = \Gamma_{Y_{2:J+1,1:T_0}^{(\bar{\mathbf{w}}, \bar{\boldsymbol{\lambda}})}, Y_{2:J+1, T_0+1:T}^{(\bar{\mathbf{w}}, \bar{\boldsymbol{\lambda}})}} \left(Y_{1,1:T_0}^{(\bar{\boldsymbol{\lambda}})} \right) \leftarrow$ the synthetic difference-in-differences unit,

where

$$Y_{2:J+1,1:T_0}^{(\bar{\mathbf{w}}, \bar{\boldsymbol{\lambda}})} = \arg \min_{\nu \in \mathcal{M}} \sum_{j=2}^{J+1} \bar{w}_j d^2(\nu, Y_{j,1:T_0}^{(\bar{\boldsymbol{\lambda}})}),$$

$$Y_{2:J+1, T_0+1:T}^{(\bar{\mathbf{w}}, \bar{\boldsymbol{\lambda}})} = \arg \min_{\nu \in \mathcal{M}} \sum_{j=2}^{J+1} \bar{w}_j d^2(\nu, Y_{j, T_0+1:T}^{(\oplus)});$$

- 4 $\tau^{(\text{GSDID})} = \gamma_{Y_{1,T_0+1:T}^{(\text{GSDID})}, Y_{1,T_0+1:T}^{(\oplus)}} \leftarrow$ the geodesic synthetic difference-in-differences estimator.
-

(GSDID). It features the geodesic synthetic control method (GSC) and the geodesic difference-in-differences model (GDID) as special cases. As we demonstrate, the proposed geodesic models can be utilized to investigate various causal effects for economically relevant outcomes that are not Euclidean such as outcomes that correspond to compositions or networks. Even for infinite-dimensional Euclidean or near-Euclidean outcomes such as functional data and distributional data the proposed GSDID model is novel and is expected to be a useful addition to the toolbox for causal analysis.

There are several directions for future research. Given a specific type of non-Euclidean outcome one often has a choice of several metrics. For example for the case of distributional outcomes, the Wasserstein metric is popular and easy to handle for one-dimensional distributions but it is very tedious to apply it for multivariate distributions (Torous et al., 2024) and alternative metrics that are easier to implement for multivariate distributions such as the Fisher-Rao metric or sliced

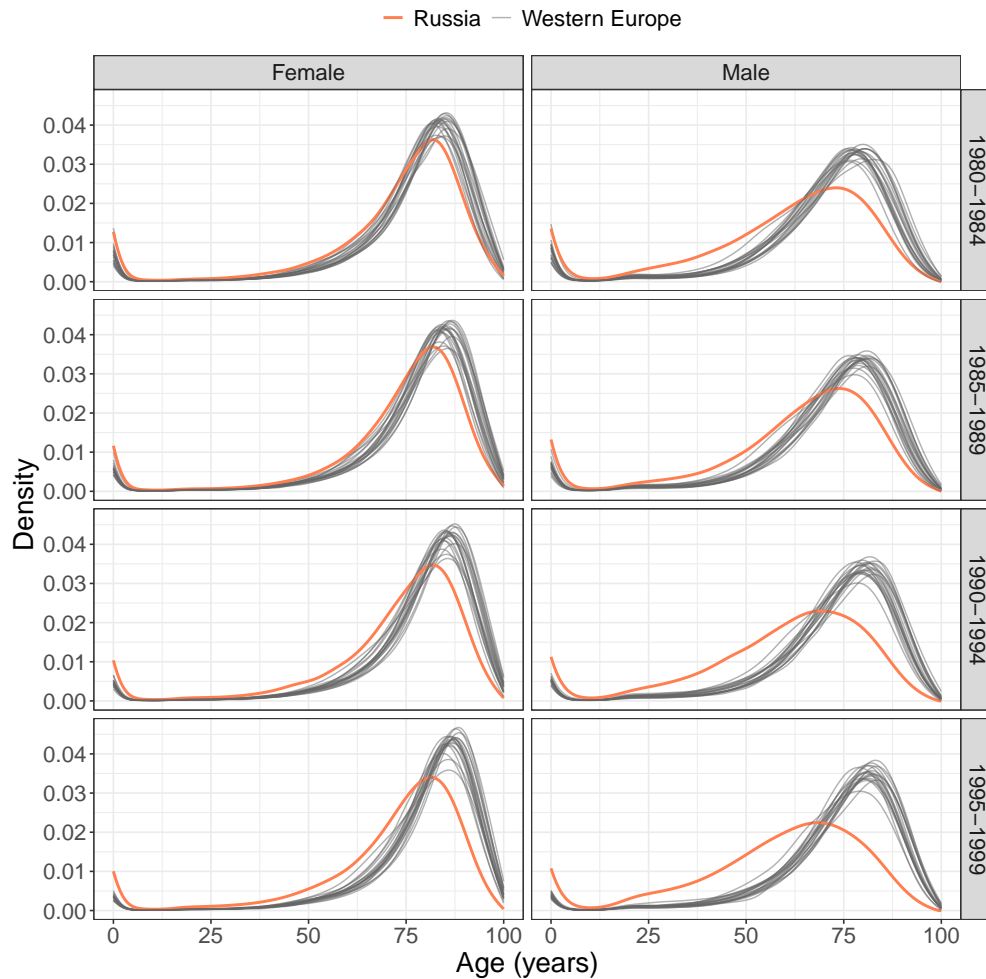


FIGURE 9. Estimated probability densities for age-at-death distributions of females (left) and males (right) for Russia (red) and Western European countries (grey) for the calendar periods 1980–1984, 1985–1989, 1990–1994, and 1995–1999.

Wasserstein metric (Bonneel et al., 2015) may sometimes be preferable. There are also many metrics available for the space of symmetric positive-definite matrices and the space of networks. The specific choice of metric could have a bearing on the results of a causal analysis. Metric selection in general and especially in a causal context remains an open problem (Dubey et al., 2024).

Furthermore, it is clearly important to further develop approaches for inference and uncertainty quantification for synthetic control models and their generalizations. One possibility to create an appropriate asymptotic framework is to extend the results of Chernozhukov et al. (2021a,b). Another promising avenue for future research is to extend the geodesic synthetic control model to the case of a staggered adoption setting (Ben-Michael et al., 2022).

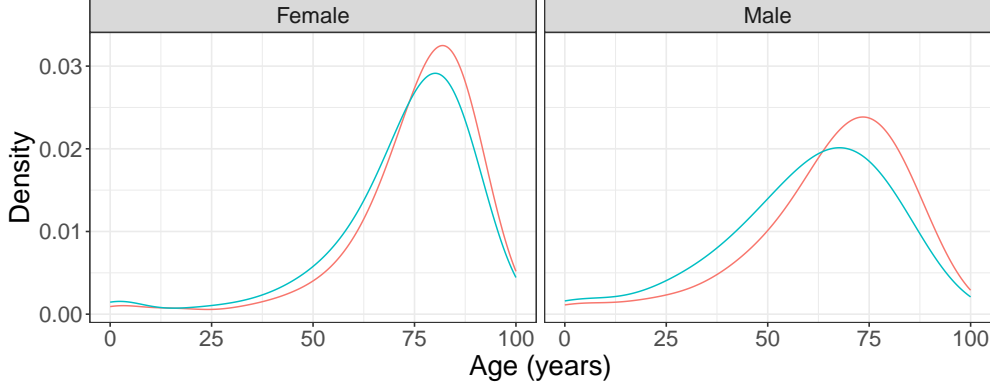


FIGURE 10. Geodesic synthetic difference-in-differences estimator for age-at-death distributions in Russia, shown separately for females (left) and males (right). The red curves represent the age-at-death density for the synthetic difference-in-differences unit, while the blue curves represent the average post-treatment age-at-death density for Russia.

APPENDIX A. VERIFICATION OF ASSUMPTION 3.1

To verify that the causal models for Examples 2.1–2.5 given in Section 2 satisfy Assumption 3.1, recall that $\bar{\mathbf{w}} \in \arg \min_{\mathbf{w} \in \Delta^{J-1}} \frac{1}{T_0} \sum_{t=1}^{T_0} d^2(Y_{1,t}, Y_{2:J+1,t}^{(\mathbf{w})})$. For $\mathbf{w} = (w_2, \dots, w_{J+1})' \in \Delta^{J-1}$, define

$$U_{2:J+1}^{(\mathbf{w})} = \arg \min_{\nu \in \mathcal{M}} \sum_{j=2}^{J+1} w_j d^2(\nu, U_j),$$

and $\mathbb{W}^* = \{\mathbf{w} \in \Delta^{J-1} : d(U_1, U_{2:J+1}^{(\mathbf{w})}) = 0\}$. Throughout Sections A.1–A.5 below, we assume that \mathbb{W}^* is not empty.

A.1. Space of networks with the Frobenius metric. Recall that $Y_{j,t}(N)$ is given as

$$\begin{aligned} Y_{j,t}(N) &= g_t(U_j) := \gamma_{\mu_t, U_j}(\alpha_t) \\ &= \mu_t + \alpha_t(U_j - \mu_t), \quad \alpha_t \in (0, 1). \end{aligned}$$

For $\mathbf{w} \in \Delta^{J-1}$,

$$\begin{aligned} U_{2:J+1}^{(\mathbf{w})} &= \sum_{j=2}^{J+1} w_j U_j, \\ g_t^{(\mathbf{w})}(U_{2:J+1}) &= \sum_{j=2}^{J+1} w_j Y_{j,t}(N) = \sum_{j=2}^{J+1} w_j \{\mu_t + \alpha_t(U_j - \mu_t)\} \\ &= \mu_t + \alpha_t \left\{ \sum_{j=2}^{J+1} w_j U_j - \mu_t \right\} = \mu_t + \alpha_t(U_{2:J+1}^{(\mathbf{w})} - \mu_t) = g_t(U_{2:J+1}^{(\mathbf{w})}). \end{aligned} \quad (\text{A.1})$$

Furthermore,

$$d_F^2(Y_{1,t}(N), Y_{2:J+1,t}^{(\mathbf{w})}) = d_F^2(g_t(U_1), g_t(U_{2:J+1}^{(\mathbf{w})}))$$

$$\begin{aligned}
&= \text{tr} \left\{ (g_t(U_1) - g_t(U_{2:J+1}^{(\mathbf{w})}))' (g_t(U_1) - g_t(U_{2:J+1}^{(\mathbf{w})})) \right\} \\
&= \alpha_t^2 \text{tr} \left\{ (U_1 - U_{2:J+1}^{(\mathbf{w})})' (U_1 - U_{2:J+1}^{(\mathbf{w})}) \right\} \\
&= \alpha_t^2 d_F^2(U_1, U_{2:J+1}^{(\mathbf{w})}), \tag{A.2}
\end{aligned}$$

where $\text{tr}(A)$ is the trace of the matrix A . This yields $\bigcap_{t=1}^{T_0} \mathbb{W}_t^* = \bigcap_{t=T_0+1}^T \mathbb{W}_t^* = \mathbb{W}^*$ and hence Assumption 3.1 holds.

A.2. Space of compositional data with the arc-length distance. Recall that $Y_{j,t}(N)$ is defined as

$$Y_{j,t}(N) = g_t(U_j) = \text{Exp}_{\mu_t}(A_t \text{Log}_{U_1}(U_j)), \quad \mu_t \in \mathcal{M}.$$

Note that $Y_{1,t} = \text{Exp}_{\mu_t}(0) = \mu_t$. Define $F_{\mathbf{w}}(\nu) = \sum_{j=2}^{J+1} w_j d^2(\nu, g_t(U_j))$, $\mathbf{w} \in \Delta^{J-1}$ and let $\text{grad}(F_{\mathbf{w}}(\nu))$ denote the gradient at $\nu \in \mathcal{M}$. Throughout we assume here that among the elements $g_t(U_2), \dots, g_t(U_{J+1})$, at least one is in the interior of \mathcal{S}_+^{d-1} . Then Theorem 1 in [Buss and Fillmore \(2001\)](#) implies that Assumption 3.1 (i) holds. For a more general discussion on sufficient conditions for the uniqueness of the Fréchet mean of a distribution on a Riemannian manifold, see Remark 2.8 in [Eltzner and Huckemann \(2019\)](#) and the references therein. For $\overline{\mathbb{W}}_t^* = \{\mathbf{w} \in \Delta^{J-1} : \sum_{j=2}^{J+1} w_j \text{Log}_{g_t(U_1)}(g_t(U_j)) = 0\}$ one can show that Assumption 3.1 (ii) holds if

$$\mathbb{W}_t^* = \overline{\mathbb{W}}_t^*. \tag{A.3}$$

Indeed, we have

$$\begin{aligned}
\mathbb{W}_t^* &= \overline{\mathbb{W}}_t^* = \left\{ \mathbf{w} \in \Delta^{J-1} : \sum_{j=2}^{J+1} w_j \text{Log}_{\mu_t} \{ \text{Exp}_{\mu_t}(A_t \text{Log}_{U_1}(U_j)) \} = 0 \right\} \\
&= \left\{ \mathbf{w} \in \Delta^{J-1} : A_t \sum_{j=2}^{J+1} w_j \text{Log}_{U_1}(U_j) = 0 \right\} \\
&= \left\{ \mathbf{w} \in \Delta^{J-1} : \sum_{j=2}^{J+1} w_j \text{Log}_{U_1}(U_j) = 0 \right\} = \mathbb{W}^*.
\end{aligned}$$

This yields $\bigcap_{t=1}^{T_0} \mathbb{W}_t^* = \bigcap_{t=T_0+1}^T \mathbb{W}_t^* = \mathbb{W}^*$ and hence Assumption 3.1 (ii) holds.

Next we show (A.3). Specifically, we establish (i) $\mathbb{W}_t^* \subset \overline{\mathbb{W}}_t^*$ and (ii) $\mathbb{W}_t^* \supset \overline{\mathbb{W}}_t^*$.

Proof of (i): Fix an arbitrary $\mathbf{w} = (w_2, \dots, w_{J+1})' \in \mathbb{W}_t^*$. By definition, $g_t^{(\mathbf{w})}(U_{2:J+1})$ is a Fréchet mean of the distribution a random element X such that $P(X = g_t(U_j)) = w_j$, $j = 2, \dots, J+1$. Further, the condition $d(g_t(U_1), g_t^{(\mathbf{w})}(U_{2:J+1})) = 0$ yields $g_t(U_1) = g_t^{(\mathbf{w})}(U_{2:J+1})$. Applying Corollary 3 in [Le and Barden \(2014\)](#), we then have $\sum_{j=2}^{J+1} w_j \text{Log}_{g_t(U_1)}(g_t(U_j)) = 0$. This implies $\mathbf{w} \in \overline{\mathbb{W}}_t^*$ and hence $\mathbb{W}_t^* \subset \overline{\mathbb{W}}_t^*$ holds.

Proof of (ii): Fix an arbitrary $\mathbf{w} = (w_2, \dots, w_{J+1})' \in \overline{\mathbb{W}}_t^*$. From the definition of $\overline{\mathbb{W}}_t^*$ and the uniqueness of the Fréchet mean, Theorem 1 in [Buss and Fillmore \(2001\)](#) yields $g_t(U_1) = g_t^{(\mathbf{w})}(U_{2:J+1})$. This implies $\mathbf{w} \in \mathbb{W}_t^*$ and hence $\mathbb{W}_t^* \supset \overline{\mathbb{W}}_t^*$.

A.3. Space of SPD matrices. First, we consider the space of SPD matrices with the Frobenius metric. Standard arguments lead to (A.1) and (A.2). Hence Assumption 3.1 holds.

Second, we consider the space of SPD matrices with the power metric family defined as

$$d_{F,p}(A, B) = \|F_p(A) - F_p(B)\|_F,$$

where $p > 0$ is a constant, $\|\cdot\|_F$ is the Frobenius metric, and F_p is a matrix power map defined as

$$F_p(A) = A^p = U\Lambda^p U' : \text{Sym}_m^+ \rightarrow \text{Sym}_m^+,$$

where $U\Lambda U'$ is the usual spectral decomposition of $A \in \text{Sym}_m^+$. The geodesic with respect to $d_{F,p}$ between A and B is given as

$$\gamma_{A,B}(t) = [A^p + t(B^p - A^p)]^{1/p} = F_{1/p}(A^p + t(B^p - A^p)).$$

Recall that $Y_{j,t}(N)$ is given as $Y_{j,t}(N) = g_t(U_j) = \gamma_{\mu_t, U_j}(\alpha_t)$. For $\mathbf{w} \in \Delta^{J-1}$,

$$(U_{2:J+1}^{(\mathbf{w})})^p = \sum_{j=2}^{J+1} w_j U_j^p,$$

$$(g_t^{(\mathbf{w})}(U_{2:J+1}))^p = \mu_t^p + \alpha_t \left\{ \sum_{j=2}^{J+1} w_j U_j^p - \mu_t^p \right\} = (g_t(U_{2:J+1}^{(\mathbf{w})}))^p.$$

Furthermore,

$$\begin{aligned} d_{F,p}^2(Y_{1,t}(N), Y_{2:J+1,t}^{(\mathbf{w})}) &= \|(Y_{1,t}(N))^p - (Y_{2:J+1,t}^{(\mathbf{w})})^p\|_F^2 = \|(g_t(U_1))^p - (g_t(U_{2:J+1}^{(\mathbf{w})}))^p\|_F^2 \\ &= \alpha_t^2 \|U_1^p - \sum_{j=2}^{J+1} w_j U_j^p\|_F^2 = \alpha_t^2 d_{F,p}^2(U_1, U_{2:J+1}^{(\mathbf{w})}). \end{aligned}$$

This yields $\bigcap_{t=1}^{T_0} \mathbb{W}_t^* = \bigcap_{t=T_0+1}^T \mathbb{W}_t^* = \mathbb{W}^*$ and hence Assumption 3.1 holds.

Third, we consider the space of SPD matrices with the Log-Euclidean metric,

$$d_{\text{LE}}(A, B) = \|\log(A) - \log(B)\|_F.$$

The geodesic with respect to d_{LE} between A and B is

$$\gamma_{A,B}(t) = \exp(\log A + t(\log B - \log A)).$$

Recall $Y_{j,t}(N) = g_t(U_j) = \gamma_{\mu_t, U_j}(\alpha_t)$. For $\mathbf{w} \in \Delta^{J-1}$,

$$\begin{aligned} \log(U_{2:J+1}^{(\mathbf{w})}) &= \sum_{j=2}^{J+1} w_j \log(U_j), \\ \log(g_t^{(\mathbf{w})}(U_{2:J+1})) &= \log(\mu_t) + \alpha_t \left(\sum_{j=2}^{J+1} w_j \log(U_j) - \log(\mu_t) \right) = \log(g_t(U_{2:J+1}^{(\mathbf{w})})). \end{aligned}$$

Further,

$$\begin{aligned} d_{\text{LE}}^2(Y_{1,t}(N), Y_{2:J+1,t}^{(\mathbf{w})}) &= \|\log(Y_{1,t}(N)) - \log(Y_{2:J+1,t}^{(\mathbf{w})})\|_F^2 = \|\log(g_t(U_1)) - \log(g_t(U_{2:J+1}^{(\mathbf{w})}))\|_F^2 \\ &= \alpha_t^2 \|\log(U_1) - \sum_{j=2}^{J+1} w_j \log(U_j)\|_F^2 = \alpha_t^2 d_{\text{LE}}^2(U_1, U_{2:J+1}^{(\mathbf{w})}). \end{aligned}$$

This yields $\bigcap_{t=1}^{T_0} \mathbb{W}_t^* = \bigcap_{t=T_0+1}^T \mathbb{W}_t^* = \mathbb{W}^*$ and hence Assumption 3.1 holds.

Fourth, we consider the space of SPD matrices with the Log-Cholesky metric. The Log-Cholesky metric is defined as

$$d_{LC}(L_1, L_2) = \left\{ \|[L_1] - [L_2]\|_F^2 + \|\log(\mathbb{D}(L_1)) - \log(\mathbb{D}(L_2))\|_F^2 \right\}^{1/2}.$$

Note that the space $(\mathcal{L}_m^+, d_{LC})$ is a geodesic metric space (Lin, 2019) and the geodesic with respect to d_{LC} between L_1 and L_2 is

$$\gamma_{L_1, L_2}(t) = [L_1] + t([L_2] - [L_1]) + \exp \{ \log(\mathbb{D}(L_1)) + t(\log(\mathbb{D}(L_2)) - \log(\mathbb{D}(L_1))) \}.$$

Let $U_j \in \mathcal{L}_m^+$, $j = 1, \dots, J+1$ and $\mu_t \in \mathcal{L}_m^+$, $t = 1, \dots, T$. Recall that $Y_{j,t}(N) = g_t(U_j) = \gamma_{\mu_t, U_j}(\alpha_t)$. For $\mathbf{w} \in \Delta^{J-1}$,

$$[U_{2:J+1}^{(\mathbf{w})}] = \sum_{j=2}^{J+1} w_j [U_j], \quad \log(\mathbb{D}(U_{2:J+1}^{(\mathbf{w})})) = \sum_{j=2}^{J+1} w_j \log(\mathbb{D}(U_j)).$$

Further,

$$[g_t^{(\mathbf{w})}(U_{2:J+1})] = [\mu_t] + \alpha_t \left\{ \sum_{j=2}^{J+1} w_j [U_j] - [\mu_t] \right\} = [g_t(U_{2:J+1}^{(\mathbf{w})})],$$

$$\log(\mathbb{D}(g_t^{(\mathbf{w})}(U_{2:J+1}))) = \log(\mathbb{D}(\mu_t)) + \alpha_t \left\{ \sum_{j=2}^{J+1} w_j \log(\mathbb{D}(U_j)) - \log(\mathbb{D}(\mu_t)) \right\} = \log(\mathbb{D}(g_t(U_{2:J+1}^{(\mathbf{w})}))).$$

Then

$$\begin{aligned} d_{LC}^2(Y_{1,t}(N), Y_{2:J+1,t}^{(\mathbf{w})}) &= \|[g_t(U_1)] - [g_t(U_{2:J+1}^{(\mathbf{w})})]\|_F^2 + \|\log(\mathbb{D}(g_t(U_1))) - \log(\mathbb{D}(g_t(U_{2:J+1}^{(\mathbf{w})})))\|_F^2 \\ &= \alpha_t^2 \left\| [U_1] - \sum_{j=2}^{J+1} w_j [U_j] \right\|_F^2 + \alpha_t^2 \left\| \log(\mathbb{D}(U_1)) - \sum_{j=2}^{J+1} w_j \log(\mathbb{D}(U_j)) \right\|_F^2 \\ &= \alpha_t^2 d_{LC}^2(U_1, U_{2:J+1}^{(\mathbf{w})}). \end{aligned}$$

This yields $\bigcap_{t=1}^{T_0} \mathbb{W}_t^* = \bigcap_{t=T_0+1}^T \mathbb{W}_t^* = \mathbb{W}^*$ and hence Assumption 3.1 holds.

A.4. Space of one-dimensional probability distributions with the 2-Wasserstein distance. Recall that $Y_{j,t}(N) = g_t(U_j) := \gamma_{\mu_t, U_j}(\alpha_t)$, $\alpha_t \in (0, 1)$. Then we have $F_{Y_{j,t}(N)}^{-1}(\cdot) = F_{\mu_t}^{-1}(\cdot) + \alpha_t(F_{U_j}^{-1}(\cdot) - F_{\mu_t}^{-1}(\cdot))$.

For $\mathbf{w} \in \Delta^{J-1}$,

$$\begin{aligned} F_{U_{2:J+1}^{(\mathbf{w})}}^{-1}(\cdot) &= \sum_{j=2}^{J+1} w_j F_{U_j}^{-1}(\cdot), \\ F_{g_t^{(\mathbf{w})}(U_{2:J+1})}^{-1}(\cdot) &= \sum_{j=2}^{J+1} w_j F_{Y_{j,t}(N)}^{-1}(\cdot) = \sum_{j=2}^{J+1} w_j \left\{ F_{\mu_t}^{-1}(\cdot) + \alpha_t(F_{U_j}^{-1}(\cdot) - F_{\mu_t}^{-1}(\cdot)) \right\} \\ &= F_{\mu_t}^{-1}(\cdot) + \alpha_t \left\{ \sum_{j=2}^{J+1} w_j F_{U_j}^{-1}(\cdot) - F_{\mu_t}^{-1}(\cdot) \right\} = \left(F_{\gamma_{\mu_t, U_{2:J+1}^{(\mathbf{w})}}(\alpha_t)} \right)^{-1}(\cdot) \\ &= F_{g_t^{(\mathbf{w})}(U_{2:J+1})}^{-1}(\cdot). \end{aligned}$$

Furthermore,

$$\begin{aligned} d_{\mathcal{W}}^2(Y_{1,t}(N), Y_{2:J+1,t}^{(\mathbf{w})}) &= d_{\mathcal{W}}^2(g_t(U_1), g_t(U_{2:J+1}^{(\mathbf{w})})) = \alpha_t^2 \int_0^1 \left\{ F_{U_1}^{-1}(p) - \sum_{j=2}^{J+1} w_j F_{U_j}^{-1}(p) \right\}^2 dp \\ &= \alpha_t^2 d_{\mathcal{W}}^2(U_1, U_{2:J+1}^{(\mathbf{w})}), \end{aligned}$$

which yields $\bigcap_{t=1}^{T_0} \mathbb{W}_t^* = \bigcap_{t=T_0+1}^T \mathbb{W}_t^* = \mathbb{W}^*$ and hence Assumption 3.1 holds.

A.5. Space of functional data with the L^2 metric. Note that

$$(Y_{j,t}(N))(s) = (\gamma_{\mu_t, U_j}(\alpha_t))(s) = \mu_t(s) + \alpha_t(U_j(s) - \mu_t(s)), \quad s \in \mathcal{T}.$$

For $\mathbf{w} \in \Delta^{J-1}$,

$$\begin{aligned} U_{2:J+1}^{(\mathbf{w})}(s) &= \sum_{j=2}^{J+1} w_j U_j(s), \\ (g_t^{(\mathbf{w})}(U_{2:J+1}))(s) &= \sum_{j=2}^{J+1} w_j (Y_{j,t}(N))(s) \\ &= \mu_t(s) + \alpha_t(U_{2:J+1}^{(\mathbf{w})}(s) - \mu_t(s)) = (g_t(U_{2:J+1}^{(\mathbf{w})}))(s), \quad s \in \mathcal{T}. \end{aligned}$$

Next,

$$\begin{aligned} d_{L^2}^2(Y_{1,t}(N), Y_{2:J+1,t}^{(\mathbf{w})}) &= d_{L^2}^2(g_t(U_1), g_t(U_{2:J+1}^{(\mathbf{w})})) = \int_{\mathcal{T}} \left\{ (g_t(U_1))(s) - (g_t(U_{2:J+1}^{(\mathbf{w})}))(s) \right\}^2 ds \\ &= \alpha_t^2 \int_{\mathcal{T}} \left\{ U_1(s) - U_{2:J+1}^{(\mathbf{w})}(s) \right\}^2 ds = \alpha_t^2 d_{L^2}^2(U_1, U_{2:J+1}^{(\mathbf{w})}), \end{aligned}$$

which gives $\bigcap_{t=1}^{T_0} \mathbb{W}_t^* = \bigcap_{t=T_0+1}^T \mathbb{W}_t^* = \mathbb{W}^*$ and hence Assumption 3.1 holds.

APPENDIX B. PROOFS

B.1. Proof of Theorem 3.1. Observe that

$$\bar{\mathbf{w}} \in \arg \min_{\mathbf{w} \in \Delta^{J-1}} \frac{1}{T_0} \sum_{t=1}^{T_0} d^2(g_t(U_1), g_t^{(\mathbf{w})}(U_{2:J+1})).$$

Then Assumption 3.1(ii) yields $\bar{\mathbf{w}} \in \bigcap_{t=T_0+1}^T \mathbb{W}_t^*$ and hence

$$Y_{1,t}^{(\text{GSC})} = g_t^{(\bar{\mathbf{w}})}(U_{2:J+1}) = g_t(U_1) = Y_{1,t}(N), \quad t = T_0 + 1, \dots, T.$$

B.2. Proof of Proposition 3.1. From the definition of the binary relation \sim on $\mathcal{G}(\mathcal{M})$, we have

$$Y_{1,t}(N) = \Gamma_{Y_{1,t}^{(\text{GSC})}, Y_{1,t}(N)}(Y_{1,t}^{(\text{GSC})}) = \Gamma_{m_t^{(\bar{\mathbf{w}})}(\mathbf{Z}_{2:J+1,1:T_0}), m_t(\mathbf{Z}_{1,1:T_0})}(Y_{1,t}^{(\text{GSC})}).$$

B.3. Proof of Theorem 6.1. Note that under Assumption 6.1, we have

$$Y_{2:J+1,1:T_0}^{(\bar{w},\bar{\lambda})} = g^{(\bar{w},\bar{\lambda})}(U_{2:J+1}, V_{1:T_0}), \quad Y_{2:J+1,T_0+1:T}^{(\bar{w},\oplus)} = g^{(\bar{w},\oplus)}(U_{2:J+1}, V_{T_0+1:T}),$$

$$Y_{1,1:T_0}^{(\bar{\lambda})} = g^{(\bar{\lambda})}(U_1, V_{1:T_0}).$$

To show (6.4) under Assumption 6.2, observe that

$$\bar{w} \in \arg \min_{w \in \Delta^{J-1}} \frac{1}{T_0} \sum_{t=1}^{T_0} d^2(g(U_1, V_t), g^{(w)}(U_{2:J+1}, V_t)).$$

This yields $\bar{w} \in \mathbb{W}_{\bar{\lambda}}^* \cap \mathbb{W}_{\oplus}^*$ and hence

$$Y_{2:J+1,1:T_0}^{(\bar{w},\bar{\lambda})} = g^{(\bar{\lambda})}(U_1, V_{1:T_0}), \quad Y_{2:J+1,T_0+1:T}^{(\bar{w},\oplus)} = g^{(\oplus)}(U_1, V_{T_0+1:T}).$$

Then we have

$$Y_{1,T_0+1:T}^{(\text{GSDID})} = \Gamma_{g^{(\bar{\lambda})}(U_1, V_{1:T_0}), g^{(\oplus)}(U_1, V_{T_0+1:T})} \left(g^{(\bar{\lambda})}(U_1, V_{1:T_0}) \right)$$

$$= g^{(\oplus)}(U_1, V_{T_0+1:T}) = Y_{1,T_0+1:T}^{(\oplus)}(N).$$

To show (6.4) under Assumption 6.3, observe that

$$\bar{\lambda} \in \arg \min_{\lambda \in \Delta^{T_0-1}} \sum_{j=2}^{J+1} d^2(g^{(\oplus)}(U_j, V_{T_0+1:T}), g^{(\lambda)}(U_j, V_{1:T_0})).$$

Then Assumption 6.3 yields $\bar{\lambda} \in \bigcap_{j=1}^{J+1} \Lambda_j^*$ and hence

$$Y_{1,T_0+1:T}^{(\text{GSDID})} = \Gamma_{g^{(\bar{w},\bar{\lambda})}(U_{2:J+1}, V_{1:T_0}), g^{(\bar{w},\oplus)}(U_{2:J+1}, V_{T_0+1:T})} \left(g^{(\bar{\lambda})}(U_1, V_{1:T_0}) \right)$$

$$= g^{(\oplus)}(U_1, V_{T_0+1:T}) = Y_{1,T_0+1:T}^{(\oplus)}(N).$$

This completes the proof.

REFERENCES

- Abadie, A. (2021). Using synthetic controls: Feasibility, data requirements, and methodological aspects. *Journal of Economic Literature*, 59(2):391–425.
- Abadie, A., Diamond, A., and Hainmueller, J. (2010). Synthetic control methods for comparative case studies: Estimating the effect of California’s tobacco control program. *Journal of the American Statistical Association*, 105(490):493–505.
- Abadie, A. and Gardeazabal, J. (2003). The economic costs of conflict: A case study of the Basque Country. *American Economic Review*, 93(1):113–132.
- Abadie, A. and L’Hour, J. (2021). A penalized synthetic control estimator for disaggregated data. *Journal of the American Statistical Association*, 116(536):1817–1834.
- Ambrosio, L., Gigli, N., and Savaré, G. (2008). *Gradient Flows in Metric Spaces and in the Space of Probability Measures*. Lectures in Mathematics. ETH Zürich. Birkhäuser Basel, 2nd edition.
- Amjad, M., Shah, D., and Shen, D. (2018). Robust synthetic control. *Journal of Machine Learning Research*, 19(22):1–51.
- Arkhangelsky, D., Athey, S., Hirshberg, D. A., Imbens, G. W., and Wager, S. (2021). Synthetic difference-in-differences. *American Economic Review*, 111(12):4088–4118.

- Arnaudon, M., Barbaresco, F., and Yang, L. (2013). Riemannian medians and means with applications to radar signal processing. *IEEE Journal of Selected Topics in Signal Processing*, 7(4):595–604.
- Arsigny, V., Fillard, P., Pennec, X., and Ayache, N. (2007). Geometric means in a novel vector space structure on symmetric positive-definite matrices. *SIAM Journal on Matrix Analysis and Applications*, 29(1):328–347.
- Ben-Michael, E., Feller, A., and Rothstein, J. (2021). The augmented synthetic control method. *Journal of the American Statistical Association*, 116(536):1789–1803.
- Ben-Michael, E., Feller, A., and Rothstein, J. (2022). Synthetic controls with staggered adoption. *Journal of the Royal Statistical Society Series B: Statistical Methodology*, 84(2):351–381.
- Billera, L. J., Holmes, S. P., and Vogtmann, K. (2001). Geometry of the space of phylogenetic trees. *Advances in Applied Mathematics*, 27(4):733–767.
- Bonneel, N., Rabin, J., Peyré, G., and Pfister, H. (2015). Sliced and Radon Wasserstein barycenters of measures. *Journal of Mathematical Imaging and Vision*, 51(1):22–45.
- Bridson, M. R. and Haefliger, A. (1999). *Metric Spaces of Non-Positive Curvature*. Grundlehren der mathematischen Wissenschaften. Springer Berlin, Heidelberg.
- Buss, S. R. and Fillmore, J. P. (2001). Spherical averages and applications to spherical splines and interpolation. *ACM Transactions on Graphics (TOG)*, 20(2):95–126.
- Büttner, T. and Lutz, W. (1990). Estimating fertility responses to policy measures in the German Democratic Republic. *Population and Development Review*, 16(3):539–555.
- Chen, K., Delicado, P., and Müller, H.-G. (2017). Modelling function-valued stochastic processes, with applications to fertility dynamics. *Journal of the Royal Statistical Society Series B: Statistical Methodology*, 79(1):177–196.
- Chen, Y., Lin, Z., and Müller, H.-G. (2023a). Wasserstein regression. *Journal of the American Statistical Association*, 118(542):869–882.
- Chen, Y., Zhou, Y., Chen, H., Gajardo, A., Fan, J., Zhong, Q., Dubey, P., Han, K., Bhattacharjee, S., Zhu, C., Iao, S. I., Kundu, P., Petersen, A., and Müller, H.-G. (2023b). *frechet: Statistical Analysis for Random Objects and Non-Euclidean Data*. R package version 0.3.0.
- Cherian, A. and Sra, S. (2016). *Positive Definite Matrices: Data representation and Applications to Computer Vision*, pages 93–114. Springer, Cham.
- Chernozhukov, V., Wüthrich, K., and Zhu, Y. (2021a). Distributional conformal prediction. *Proceedings of the National Academy of Sciences*, 118(48):e2107794118.
- Chernozhukov, V., Wüthrich, K., and Zhu, Y. (2021b). An exact and robust conformal inference method for counterfactual and synthetic controls. *Journal of the American Statistical Association*, 116(536):1849–1864.
- Dai, X., Lin, Z., and Müller, H.-G. (2021). Modeling sparse longitudinal data on Riemannian manifolds. *Biometrics*, 77(77):1328–1341.
- Dryden, I. L., Koloydenko, A., and Zhou, D. (2009). Non-Euclidean statistics for covariance matrices, with applications to diffusion tensor imaging. *Annals of Applied Statistics*, 3(3):1102–1123.
- Dubey, P., Chen, Y., and Müller, H.-G. (2024). Metric statistics: Exploration and inference for random objects with distance profiles. *Annals of Statistics*, 52(2):757–792.
- Eltzner, B. and Huckemann, S. F. (2019). A smeary central limit theorem for manifolds with application to high-dimensional spheres. *Annals of Statistics*, 47(6):3360–3381.

- Fréchet, M. (1948). Les éléments aléatoires de nature quelconque dans un espace distancié. *Annales de l'Institut Henri Poincaré*, 10(4):215–310.
- Ginestet, C. E., Simmons, A., and Kolaczyk, E. D. (2012). Weighted Fréchet means as convex combinations in metric spaces: properties and generalized median inequalities. *Statistics and Probability Letters*, 82(10):1859–1863.
- Gunsilius, F., Hsieh, M. H., and Lee, M. J. (2024). Tangential Wasserstein projections. *Journal of Machine Learning Research*, 25(69):1–41.
- Gunsilius, F. F. (2023). Distributional synthetic controls. *Econometrica*, 91(3):1105–1117.
- Hsing, T. and Eubank, R. (2015). *Theoretical Foundations of Functional Data Analysis, with an Introduction to Linear Operators*, volume 997. John Wiley & Sons.
- Human Fertility Database (2025). Max Planck Institute for Demographic Research (Germany) and Vienna Institute of Demography (Austria). Available at www.humanfertility.org (data downloaded on March 16, 2025).
- Human Mortality Database (2024). Max Planck Institute for Demographic Research (Germany), University of California, Berkeley (USA), and French Institute for Demographic Studies (France). Available at www.mortality.org (data downloaded on September 13, 2024).
- Johnson, S. G. (2008). *The NLOpt nonlinear-optimization package*.
- Kolaczyk, E. D. and Csárdi, G. (2014). *Statistical Analysis of Network Data with R*, volume 65. Springer New York.
- Kurisu, D., Zhou, Y., Otsu, T., and Müller, H.-G. (2024). Geodesic causal inference. *arXiv preprint arXiv:2406.19604*.
- Le, H. and Barden, D. (2014). On the measure of the cut locus of a Fréchet mean. *Bulletin of the London Mathematical Society*, 46(4):698–708.
- Lin, Z. (2019). Riemannian geometry of symmetric positive definite matrices via Cholesky decomposition. *SIAM Journal on Matrix Analysis and Applications*, 40(4):1353–1370.
- Lin, Z., Kong, D., and Wang, L. (2023). Causal inference on distribution functions. *Journal of the Royal Statistical Society Series B: Statistical Methodology*, 85(2):378–398.
- Lin, Z. and Yao, F. (2019). Intrinsic Riemannian Functional data analysis. *Annals of Statistics*, 47(6):3533–3577.
- McCann, R. J. (1997). A convexity principle for interacting gases. *Advances in Mathematics*, 128(1):153–179.
- Notzon, F. C., Komarov, Y. M., Ermakov, S. P., Sempos, C. T., Marks, J. S., and Sempos, E. V. (1998). Causes of declining life expectancy in Russia. *JAMA*, 279(10):793–800.
- Panaretos, V. M. and Zemel, Y. (2020). *An Invitation to Statistics in Wasserstein Space*. Springer New York.
- Patrangenaru, V. and Ellingson, L. (2015). *Nonparametric Statistics on Manifolds and Their Applications to Object Data Analysis*. CRC Press.
- Petersen, A. and Müller, H.-G. (2016). Functional data analysis for density functions by transformation to a Hilbert space. *Annals of Statistics*, 44(1):183–218.
- Petersen, A. and Müller, H.-G. (2019). Fréchet regression for random objects with Euclidean predictors. *Annals of Statistics*, 47(2):691–719.
- Petersen, A., Zhang, C., and Kokoszka, P. (2022). Modeling probability density functions as data objects. *Econometrics and Statistics*, 21:159–178.

- Powell, M. J. D. (1994). *A Direct Search Optimization Method That Models the Objective and Constraint Functions by Linear Interpolation*, pages 51–67. Springer Netherlands, Dordrecht.
- Ramsay, J. O. and Silverman, B. W. (2005). *Functional Data Analysis*. Springer Series in Statistics. Springer New York, 2nd edition.
- Robbins, M. W., Saunders, J., and Kilmer, B. (2017). A framework for synthetic control methods with high-dimensional, micro-level data: Evaluating a neighborhood-specific crime intervention. *Journal of the American Statistical Association*, 112(517):109–126.
- Scealy, J. and Welsh, A. (2011). Regression for compositional data by using distributions defined on the hypersphere. *Journal of the Royal Statistical Society Series B: Statistical Methodology*, 73(3):351–375.
- Severn, K. E., Dryden, I. L., and Preston, S. P. (2022). Manifold valued data analysis of samples of networks, with applications in corpus linguistics. *Annals of Applied Statistics*, 16(1):368–390.
- Stellato, B., Banjac, G., Goulart, P., Bemporad, A., and Boyd, S. (2020). OSQP: An operator splitting solver for quadratic programs. *Mathematical Programming Computation*, 12(4):637–672.
- Torous, W., Gunsilius, F., and Rigollet, P. (2024). An optimal transport approach to estimating causal effects via nonlinear difference-in-differences. *Journal of Causal Inference*, 12(1):20230004.
- Van Dijcke, D. (2025). Regression discontinuity design with distribution-valued outcomes. *arXiv preprint arXiv:2504.03992*.
- Wang, J.-L., Chiou, J.-M., and Müller, H.-G. (2016). Functional Data Analysis. *Annual Review of Statistics and its Application*, 3:257–295.
- Yuan, Y., Zhu, H., Lin, W., and Marron, J. (2012). Local polynomial regression for symmetric positive definite matrices. *Journal of the Royal Statistical Society Series B: Statistical Methodology*, 74(4):697–719.
- Zhou, Y., Kurisu, D., Otsu, T., and Müller, H.-G. (2025). Geodesic difference-in-differences. *arXiv:2501.17436*.
- Zhou, Y. and Müller, H.-G. (2022). Network regression with graph Laplacians. *Journal of Machine Learning Research*, 23(320):1–41.
- Zhu, C. and Müller, H.-G. (2023). Geodesic optimal transport regression. *arXiv preprint arXiv:2312.15376*.

(D. Kurisu) CENTER FOR SPATIAL INFORMATION SCIENCE, THE UNIVERSITY OF TOKYO, 5-1-5, KASHIWANOHA, KASHIWA-SHI, CHIBA 277-8568, JAPAN.

Email address: `daisukekurisu@csis.u-tokyo.ac.jp`

(Y. Zhou) DEPARTMENT OF STATISTICS, UNIVERSITY OF CALIFORNIA, DAVIS, ONE SHIELDS AVENUE, DAVIS, CA, 95616, USA.

Email address: `ydzhou@ucdavis.edu`

(T. Otsu) DEPARTMENT OF ECONOMICS, LONDON SCHOOL OF ECONOMICS, HOUGHTON STREET, LONDON, WC2A 2AE, UK.

Email address: `t.otsu@lse.ac.uk`

(H.-G. Müller) DEPARTMENT OF STATISTICS, UNIVERSITY OF CALIFORNIA, DAVIS, ONE SHIELDS AVENUE, DAVIS, CA, 95616, USA.

Email address: `hgmueeller@ucdavis.edu`